DENSITY FUNCTIONAL THEORY STUDY OF ADSORPTION OF CROCONATE DYES ON TiO_2 ANATASE (010) AND (100) SURFACES

BY

RANWAHA TSHIFHIWA STEVEN

(11612891)

DISSERTATION

PRESENTED IN PARTIAL FULFILMENT FOR THE REQUIERENTS OF THE MASTERS (MSc) OF SCIENCES DEGREE IN PHYSICS

AT THE

SCHOOL OF MATHEMATICS AND NATURAL SCIENCES

UNIVERSITY OF VENDA

SUPERVISOR: DR N E MALUTA (UNIVEN)

CO-SUPERVISOR: PROF R R MAPHANGA (CSIR)

YEAR: 2018

DECLARATION

I Ranwaha Tshifhiwa Steven, declare that this research report submitted to the University of Venda titled "**Density functional theory study of adsorption of croconate dyes on TiO_2 anatase 010 and 100 surfaces**" for the M.Sc degree in physics is my original work and has not been submitted for any degree at this or any other institution. The report does not contain other persons' writing unless specifically acknowledged and referenced accordingly.

Signed (student): …… at……..
On……day of…. …….

DEDICATIONS

I would like to dedicate this dissertation to my family for their moral support throughout my studies. Above all I would love to dedicate this to almighty God for His daily support and protection.

ACKNOWLEDGEMENTS

I would love to extend my gratitude to my supervisor DR N E Maluta and Co-Supervisor Prof R R Maphanga for helping me throughout this research. I would also want to extend my gratitude to the University of Venda department of Physics for opportunity to proceed with my M.Sc. studies. Lastly, I would like to acknowledge the National Research Foundation (NRF) for financial support.

ABSTRACT

Currently the dye sensitized solar cells have attracted more attention due to their low cost, transparency and flexibility. These types of solar cells use the dye molecule adsorbed on TiO_2 semiconductor in Nano architecture with the role of absorbing photons, in recent research attempts are being made to shifts the absorption spectral of TiO_2 to visible and near infrared–region of solar spectrum to achieve maximum photo absorption which yields to an increase in the efficiency of the dye sensitized solar cells.

In the current study, density functional theory (DFT) was used to model two croconate dyes (CR1 and CR2), one with an electron donating methyl group (CR1) and the other with an electron –withdrawing caboxyl group (CR2). The geometric, electronic and optical properties of these dyes were compared. The adsorption behaviour of the two dyes on (010 and 100) anatase TiO_2 surfaces were investigated in this study by employing first principle calculation based on DFT using a plane-wave pseudo potential method. The generalized gradient approximation (GGA) was used in the scheme of Perdew-Burke Ernzerhof to describe the exchange -correlation function as implemented in the CASTEP package in Material Studio of BIOVIA. The adsorption results shows a spontaneous electron injection followed by efficient regeneration of the oxidized dye molecules by the electrolyte and strong binding ability of CR2 to the TiO_2 surface, but also shows a comparable binding strength of CR1. The results of this study will help in the design of high efficient dye for DSSCs.

Keywords: Dye sensitized solar cells, Dye, Croconate, Efficiency

LIST OF ABBREVIATIONS

PV	=	Photovoltaic
DSSCs	=	Dye-Sensitized Solar Cells
TiO_2	=	Titanium Dioxide
UV	=	Ultraviolet
VB	=	Valence Band
CB	=	Conduction Band
DOS	=	Density of States
PDOS	=	Partial Density of States
DFT	=	Density Functional Theory
LDA	=	Local Density Approximation
GGA	=	Generalized Gradient Approximation
CASTEP	=	Cambridge Sequential Total Energy Package
TCO	=	Transparent Conductive Oxide
VAMP	=	Vulnerability Assessment Management Program
EDFT	=	Ensemble density functional theory
TiO_2	=	Titanium Dioxide
E_g	=	Energy Gap
TMA	=	Trimethylamine
LSDA	=	Local Spin Density Approximation
HEG	=	Homogeneous Electron Gas
XC	=	Exchange Correlation
PSPW	=	Pseudopotential Plane Wave
LAPW	=	Linearized Augmented Plane Wave

PAW	=	Projector Augmented Wave
PBE	=	Perdew-Burke Ernzerhof

LIST OF FIGURES

FIGURE PAGE

LIST OF TABLES

TABLE PAGE

TABLE OF CONTENTS

1. CHAPTER 1

1.1. General Introduction

Availability of energy and energy distribution is one major challenge being faced globally today [1]. This challenge is faced by both developed and developing countries, and South Africa is not an exception. For instance, South African institutions, health care centers, industries, companies and all other sources of basic needs require electricity to operate optimally on daily basis. The economy of most developing countries such as South Africa depends on mines and manufacturing industries, which require huge amount of energy to function properly. Like many other developed and developing countries, SA energy demand is increasing continuously. The energy demand is high such that the country was faced with load shedding blackouts few years ago and most recently. Thus, the source and supplier of electricity in SA is failing to meet the demand.

South Africa as a country has one major supplier of electricity called Eskom. Almost 80% of power generated by Eskom comes from coal, which is a non-renewable source of energy that is becoming depleted each and every day [2]. It is very well understood worldwide that the fossil fuels will be depleted in the near future and Renewable energy technologies as an alternative sources of energy supply are been proposed as a solution to the problem [2]. Different renewable energy technologies are being investigated and developed to increase the supply of energy. Amongst those various technologies, solar energy technologies are regarded as the most promising technology to solve energy crisis globally. There are many energy technologies that are being researched and developed, one of these technologies includes; nuclear energy and renewable solar energy, wind energy, hydro energy, biogas, etc. [1,2]. However, nuclear energy relies on finite sources and involves significant problems [3]. The challenge with hydro energy for SA is that there are no big rivers in the country, hence hydroelectricity is not a choice of energy supply in SA. The main hydro supply of electricity is imported by Eskom from a neighboring country Mozambique.

The earth receives an incredible supply of solar energy. The sun, an average star, is a fusion reactor that has been burning for over 4 billion years. It provides enough

energy in one minute to supply the world's energy needs for one year. In one day, it provides more energy than our current population would consume in 27 years [4]. The amount of solar radiation striking the earth over a three-day period is equivalent to the energy stored in all fossil energy sources [5]. Solar energy is free, inexhaustible resource, yet harnessing it is a relatively new idea. There are several advantages of photovoltaic solar power that make it "one of the most promising renewable energy sources in the world." It is non-polluting, has no moving parts that could break down, requires little maintenance and no supervision, and has a lifespan of 20-30 years with low running costs [6]. It is especially unique because no large-scale installation is required. Remote areas can easily produce their own supply of electricity by constructing small or large systems as needed. Solar power generators can be simply distributed to homes, schools, or businesses, where their assembly requires no extra development or land area and their operation is safe and quiet. The amount of sunlight a location receives varies greatly depending on geographical location, time of day, season and clouds.

Considering the importance of the use of solar cells and efficient use of solar energy; a solar cell or photovoltaic cell is an electrical device that converts the energy of light directly into electricity by the photovoltaic effect, which is a physical and chemical phenomenon [6]. It is a form of photoelectric cell or a device, whose electrical characteristics such as current, voltage, or resistance, vary when exposed to light. Solar cells are the building blocks of photovoltaic modules. Solar cells are described as being photovoltaic irrespective of whether the source is sunlight or an artificial light. They can also be used as a photo detector (for example infrared detectors), detecting light or other electromagnetic radiation near the visible range, or measuring light intensity [5, 6].

In this study computational simulation techniques were used to investigate the properties of TiO_2 semiconductor as a material used in dye-sensitized solar cells (DSSCs).DSSCs are regarded as the most promising technology that could revolutionize global energy crisis due their low cost, transparency and flexibility. These types of solar cells harness the energy by adsorbing dye molecules on top of TiO_2 semiconductor. Hence, the current study specifically uses computer modelling techniques to investigate electrical and optical properties of croconate dye molecules with small HOMO-LUMO gap adsorbed on TiO_2 anatase surfaces.

1.2. Photovoltaic Cells

A photovoltaic (PV) cell is a specialized semiconductor diode that converts visible light into direct current (DC). Some PV cells can also convert infrared (IR) or ultraviolet (UV) radiation into DC electricity. Photovoltaic cells are an integral part of solar-electric energy systems, which are becoming increasingly important as alternative sources of utility power [4].

Large sets of PV cells can be connected together to form solar modules, arrays, or panels. The use of PV cells and batteries for the generation of usable electrical energy is known as photovoltaics. One of the major advantages of photovoltaics is the fact that it is non-polluting, requiring only real estate (and a reasonably sunny climate) in order to function. Another advantage is that the solar energy is unlimited. Once a photovoltaic system has been installed, it can provide energy at essentially no cost for years, and with minimal maintenance [4, 7].

Solar cells can be classified into first, second and third generation. The first-generation cells are called conventional, traditional or wafer-based cells, made by crystalline silicon. These are the commercially predominant PV technologies that includes materials such as polysilicon and monocrystalline silicon. The first PV cells were made of silicon combined, or doped, with other elements to affect the behavior of electrons or holes (electron absences within atoms). Second generation cells are thin film solar cells, which include amorphous silicon, cadmium telluride (CdTe) and copper indium gallium selenide (CIGS) and are commercially significant in utility-scale photovoltaic power stations, building integrated photovoltaics or in small stand-alone power system. The third generation of solar cells includes a number of thin-film technologies often described as emerging photovoltaics. Most of the 3rd generation solar cells have not yet been commercialized and are still in the research and development phase. Many use organic materials, often organometallic compounds as well as inorganic substances. Despite the fact that their efficiencies had been low and the stability of the absorber material was often too short for commercial applications, there is a lot of research activities invested into this technology as it is promising to achieve the goal of producing low-cost and high-efficient solar cells [6].

As illustrated above solar cells are different and classified into the different generations, and these generations are named after the semiconducting material used to manufacture them. The semiconductor must have certain characteristics in order to absorb sunlight. Some cells are designed to handle sunlight that reaches the earth's surface, while others are optimized for use in space [7]. Solar cells can be made of only one single layer of light-absorbing material (single-junction) or use multiple physical configurations (multi-junctions) to take advantage of various absorption and charge separation mechanisms.

1.3. Dye Sensitized Solar Cells

The dye sensitized solar cell is based on a semiconductor formed between a photo-sensitized anode and an electrolyte which is a photo electrochemical system [8] The DSSCs have a number of attractive features; (i) it is simple to manufacture, using conventional roll-printing techniques, (ii) it is semi-flexible and semi-transparent, which offers a variety of uses not applicable to glass-based systems, and (iii) most of the materials used are of low cost. In practice it has proven difficult to eliminate a number of expensive materials, notably platinum and ruthenium [7, 8]. The liquid electrolyte presents a serious challenge to making a cell suitable for use in all weather conditions. Although its conversion efficiency is less than the best thin-film cells, in theory its price/performance ratio should be good enough to allow it to compete with fossil fuel electrical generation by achieving grid parity. Commercial applications, which were held up due to chemical stability problems [2,5] are forecast in the European Union Photovoltaic Roadmap to significantly contribute to renewable electricity generation by 2020 [8].

Dye sensitized solar cells also referred to as dye sensitized cells (DSSCs), are a third generation photovoltaic cells that convert any visible light into electrical energy. This new class of advanced solar cells can be likened to artificial photosynthesis due to the way in which it mimics nature’s absorption of light energy. DSSCs were invented in 1991 by Professor Michael Gräetzel and Dr Brian O’Regan at École Polytechnique Fédérale de Lausanne (EPFL) in Switzerland and are often referred to as the Gräetzel cell. DSSC is a disruptive technology that can be used to produce electricity in a wide range of light conditions, indoors and outdoors, enabling the user to convert both

artificial and natural light into energy to power a broad range of electronic devices. DSSCs are of low-cost solar cells belonging to the group of thin film solar cells [5, 6].

Other materials, such as copper indium diselenide (CIS), cadmium telluride (CdTe), and gallium arsenide (GaAs), have been developed for use in PV cells. There are two basic types of semiconductor material, namely positive (or p-type) and negative (or n-type) materials. In a PV cell, flat pieces of these materials are placed together, and the physical boundary between them is called the p-n junction. The device is constructed in such a way that the junction can be exposed to visible light, IR, or UV. When such radiation strikes the p-n junction, a voltage difference is produced between the p-type and n-type materials. Electrodes connected to the semiconductor layers allow current to be drawn from the device [7].

DSSCs is a type of photo electrochemical cell which look like a sandwich structure, whose working principle is based on photovoltaic effect, having a photo electrode which combines semiconductor material typically TiO_2 and sensitized dye molecule. The photo electrode and catalytic counter electrode are deposited onto transparent conducting material. Electrolyte is the combination of organic and inorganic material (inorganic salts, redox couple, and type semiconductor, conducting polymers) [6]. Electrical energy is generated from photo-electrode. The dye molecules act as a sensitizers and absorb the photon from the sun and they then inject an electron to the semiconductor. Then the transparent conducting material transports the electron to counter electrode among outer circuit. The dye is then oxidized to ground state and again regenerates through the electrolyte. The role of electrolyte is the reduction of the oxidized dye molecule for continuous electron production and electrolyte regenerate itself, getting electron from outer circuit along with counter electrode [8].

The working principle of DSSCs shown if Figure 1.1 is based on the electron transport and adsorption at visible light by mimicking photosynthesis process, which is natural process were plants convert sunlight into energy. This is done by sensitizing a monocrystalline TiO_2 film, using different organic or inorganic dye molecules [9, 10]. In a dye sensitized molecule solar cell, charge separation is accomplished by kinetic competition like in photosynthesis, leading to photovoltaic action [11]. As these type of solar cells are mimic the photosynthesis, there is limitation on its efficiency and

other properties that determine the efficiency,for example, most of the typically used dye molecules have poor absorption in the red part of the spectrum compared to silicon. These are some of factors that limit the current generated by a DSSC and for comparison, a traditional silicon-based solar cell offers about 35 mA/cm^2, whereas current DSSCs offer about 20 mA/cm^2.

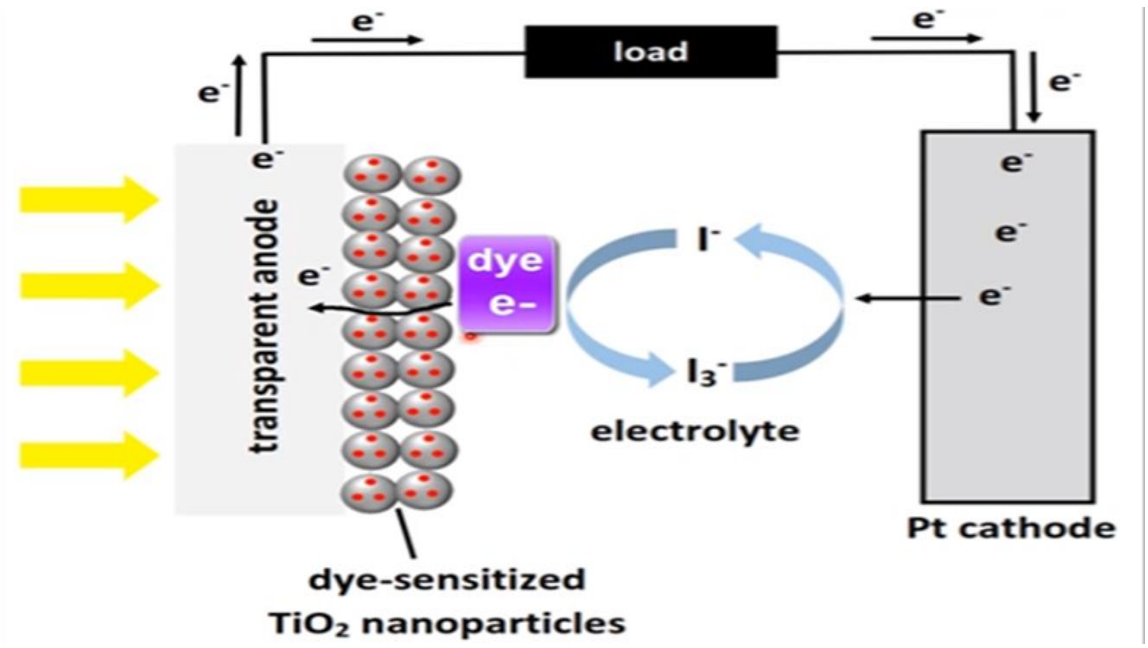

Figure 1.1: working principle of DSSCs [12]

Major difference between DSSCs and other semiconductor solar cells is that the solar light is not mainly absorbed by the semiconductor TiO_2, and the electron-hole pair is separated by the built-in-potential of a p-n junction. A visible component of the solar light generates electron-hole pairs in the dye sensitizer which anchors on the photo anode of wide band gap semiconductor nanoparticles. When the electron-hole pairs are formed in the dye molecules, they are quickly separated at a picosecond scale due to the difference in energy levels. Electrons are injected from the dye to the conduction band of the photo anode and are transferred to the transparent conducting oxide film that is coated on the glass. Holes in the dye molecules are delivered to the electrolyte through a redox reaction. [12].

Thus, several problems remain to be solved in the development of the DSSCs for a large-scale application [13, 14]. There are fundamental research issues such as the origin of the moderate efficiency, which is presently approximated as 15%, factors affecting the efficiency, extending of photon absorption to visible and infrared region, etc. [14].

1.4. Dye Molecules

As a major component, the dye absorb incoming solar light to generate electron/hole pairs. The role of the sensitizer requires that it matches well the energy level, to facilitate efficient electron injection and dye regeneration, strong physical anchoring to photo anode, sufficient absorption of solar light, and stable operation for a long period [14]. Metal-complex, metal-free organic dye, natural dye, and quantum dot have been used as sensitizing materials [14]. The widely used sensitizer is polypyridyl complex of ruthenium because of its high efficiency and long term stability; N3 and N719 are typical examples. Black dye extends the light absorption to near IR range, and amphiphilic Z907 shows higher stability at high temperature application. Organic dye is an emerging sensitizer because of tunable band gap, large extinction coefficient, and relatively cheaper cost [15].

The organic dyes such as coumarins, merocyanine, hemicyanine, indoline, squaraines, and croconates are receiving an interest as light harvesting materials, because of their relatively cheap cost, easy to synthesize and environmental friendliness [13]. Interestingly, croconate dyes have narrow and intense absorption bands in the near infrared (NIR) region, and can absorb light even at higher wavelengths than ruthenium based metal dyes [13].

1.5. Titanium Dioxide

Titanium dioxide (TiO_2) is an effective semiconductor, low in cost, available in large quantity and not harmful or toxic to living tissue [3]. Its applications diversified over the last few decades, including but not limited to biological implants, photo catalysis, commercial products such as sunscreens and toothpastes, small industrial products such as paints, lacquers and paper, and in photocatalytic processes such as water treatment [9]. TiO_2 absorbs light in the ultraviolet spectrum but can be photosensitized by the adsorption of organic and/or inorganic dye molecules to absorb the light in visible and near infrared regions. The large band gap properties, in addition to its abundance, low cost, stability and low toxicity are the basis for its application in solar cells,TiO_2 is a good electron and hole donor and can therefore, promote photocatalytic processes at its interface [10].

1.6. Aim and Objectives

1.6.1. Aim

The aim of this study was to use computer simulation methods to investigate the characteristics of dye molecules adsorbed onto anatase TiO_2. (100) and (010) surfaces

1.6.2. Objectives

The objectives of this study were to:

- Determine the UV-Vis of the croconates dye molecules
- Calculate the light harvesting efficiency of croconate dyes
- Calculate optical absorption of croconate dyes
- Calculate the HOMO-LUMO gap of the croconate dye molecules
- Determine the adsorption energy between the dye molecules and the surfaces
- Calculate the electron injection between dye molecules adsorbed on anatase TiO_2 (100) and (010) surfaces.

2. CHAPTER 2 LITERATURE REVIEW

2.1. TiO_2 Band Gap

The measurement of the band gap of materials is important in semiconductor, nanomaterial and solar industries. The band gap of a material can be determined from its UV absorption spectrum [15]. The band gap is important as it determines the portion of the solar spectrum a photovoltaic cell absorbs [16]. Much of the solar radiation reaching the earth is comprised of wavelengths with energies greater than the band gap of silicon [17]. These higher energies are absorbed by the solar cell, but the difference in energy is converted into heat rather than usable electrical energy. Consequently, unless the band gap is controlled, the efficiency of the solar cell will be poor. Using layers of different materials with different band gap properties has been proven to maximize the efficiency of solar cells [17]. In the semiconductor and nanomaterial industries, titanium dioxide is added as an ingredient to coatings. TiO_2 is thought to promote the internal trapping of light by scattering the light reflected from the metallic electrode in the active layer and also to improve the transport of charge carriers through the active layer [17].

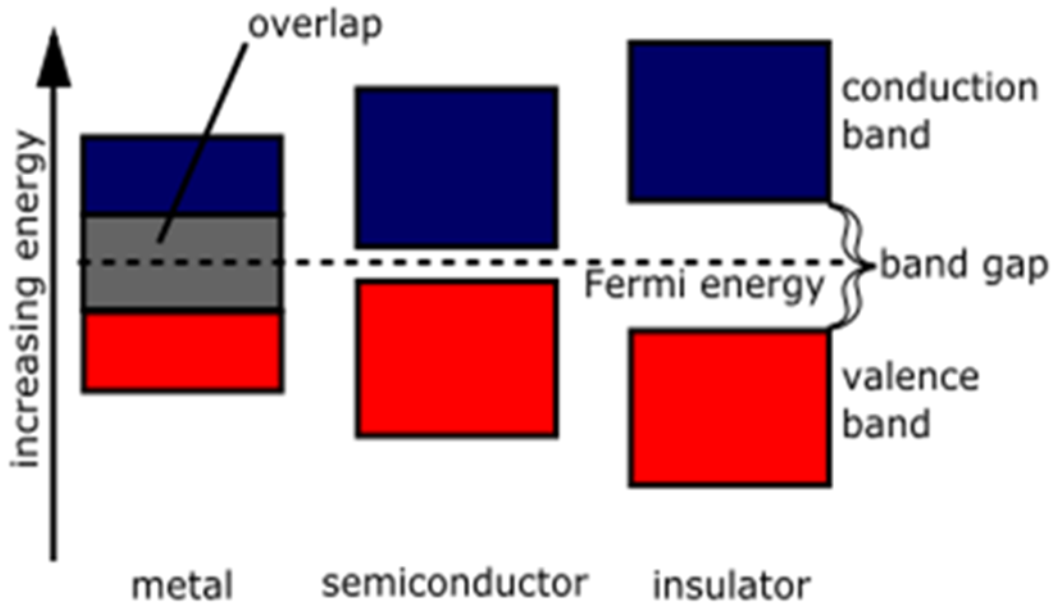

Figure 2.1: Illustration of band structure of different materials [17]

The term “band gap” refers to the energy difference between the top of the valence band to the bottom of the conduction band as depicted in Figure 2.1, under light illumination the electrons are able to jump from one band to another. In order for an electron to jump from a valence band to a conduction band, it requires a specific minimum amount of energy for the transition that is the band gap energy [17].

TiO_2 has been used in photocatalysis and in photovoltaics due to its far reaching mix of energy band structure, carrier transport, and dormancy [18]. The 3.2 eV band gap of anatase TiO_2 demonstrates its low efficiency in its application in PV technologies. The solution to this low efficiency problem is to use full range of sun based light, and the band gap engineering. In particular, nitrogen doping, iron doping, and N/Fe codoping were examined for their photocatalytic impact. Han *et al*. [19] investigated both N and Fe doping and they appear to narrow the band gap of the TiO_2. N-doping upgrades its unmistakable light photocatalytic execution, while Fe-doping and codoping resulted in a poor photocatalysis. Low temperature fluorescence spectra showed the high recombination in Fe-doped and co-doped samples.

Consolidating band gap engineering (doping) and transport on doped nanorods were examined by Han *et al.* [19] it was observed that Nb doped nanorods demonstrated a higher conductivity, a superior back contact amongst (fluorine-doped tin oxide) FTO. Its advantage is a simple infusion of electron from dye sensitizers to nanorods, and thus, a less recombination.

De Lazaro *et al.* [20] investigated structural and electronic properties of S and Mo doped TiO_2 anatase using framework of periodic calculations with the inclusion of DFT-D2 dispersion potential adjusted for this system (B3LYP-D*). The role of dispersion in distorted unit cells was evaluated in terms of lattice parameters, elastic constants, equation of state, vibrational properties, and electronic properties (band structure and density of states). A more reliable description at high pressures was achieved because the B3LYP-D* presented an improvement in all properties for undistorted bulk over conventional B3LYP and B3LYP-DThe studied distortions gave insight into behavior of electronic and structural properties of bulk anatase TiO_2 due to local stress induced by doping, defects and physical tensions in nanometric forms.

Long *et al.* [21] explored the electronic properties and photocatalytic activity of X (N, C)/transition metal and (TM=Ta, Hf, Fe) - codoped anatase TiO_2 utilizing density functional theory. The study demonstrated that only the (N, Ta) - codoping case limits the band gap fundamentally by around 0.48 eV, driven by the continuum-like p–d hybridized states above the highest point of valence band and d-states at the base of conduction band. The calculated energy results propose that codoping of Ta with N can build the N fixation in N-doped TiO_2 based on energy results.

2.2. TiO_2 Anatase

Titanium dioxide also known as titania, is the naturally occurring oxide of titanium. It is a versatile transition-metal oxide and a useful material in various present and future applications related to catalysis, electronics, photonics, sensing, medicine, and controlled drug release. Furthermore, it has more applications in various industries such as aerospace, sports, medicine, paint (to give high gloss, rich depth of color and to replace metal lead), food (to increase the shelf life of products) and cosmetics (UV protection in sunscreens and many other products) [10, 22]. Titania has been extensively studied owing to its physical and chemical properties in photo-catalytic applications for environmental remediation. It is usually used in the form of nanoparticles in suspension for high catalytic surface area and activity. It occurs in nature in three commonly known phases, i.e.; anatase, brookite and rutile forms. These phases are characterized with high refractive index (anatase = 2.488, rutile = 2.609, brookite = 2.583), low absorption and low dispersion in visible and near-infrared spectral regions, high chemical and thermal stabilities [22]. In particular, anatase phase is considered for various applications including lithium-ion batteries, filters, anti-reflective and high reflective coatings and has been widely investigated. But, it still remains a challenge to keep this phase stable from easy transformation to rutile phase.

Anatase and rutile have a similar symmetry, tetragonal 4/m 2/m 2/m, in spite of having distinctive structures. In rutile, the structure depends on octahedrons of titanium oxide which impart two edges of the octahedron to different octahedrons and frame chains. It is the chains themselves which are masterminded into a four-overlay symmetry. In anatase, the octahedrons share four edges consequently the four overlap axis [16].

Crystals of anatase are extremely particular and are not effortlessly mistook for some other mineral, they frame the eight confronted tetragonal dipyramids that come to sharp extended points [16]. The extension is sufficiently professed to recognize this precious stone frame from octahedral crystals, yet there is a closeness [16]. In reality anatase is wrongly called "octahedrite" regardless of the distinction in structures. Pleasant examples of anatase are connected with quartz and are considered works of art in the mineral world. The great brilliance, very much framed crystal shape and interesting character make anatase a prevalent mineral for gatherers [13].Chen *et al*.

[11] Investigated TiO_2 as a promising photo-catalyst and highlighted the role that it can play in alleviating environmental and pollution challenges. It is widely used as a photo-catalyst due to its relatively cheap cost, non-toxicity and high chemical stability.

TiO_2 has unique properties that advance the current technology in the fields of catalysis, solar cell, energy storage, and semiconductor devices. However, there are several issues to be addressed to maximize the potential technological use of TiO_2. For example the band gap of TiO_2 is not suitable in harnessing the full spectrum of solar spectrum. Light absorption of TiO_2 is an important process for solar light related application especially in photocatalysis. The wide band gap property of TiO_2 implies that its light absorption is limited in UV and lower wavelength than UV [23]. In dye sensitized solar cell, the conduction band edge of TiO_2 needs to be lower than the lowest unoccupied molecular orbital (LUMO) of the dye sensitizer for efficient electron injection, while extremely low conduction band edge decreases the open circuit voltage. Hence, it is of importance to control and modify band edge position to achieve an optimum output.

The doping of TiO_2 anatase with different metals has been investigated in recent years as a way of improving its performance in photocatalysis and solar cells, The results shows that the absorption efficiency of TiO_2 can be tuned into the visible-light range by substituting the Ti atoms with the alkali-earth metal atom, in which the strong peak of red-light absorption is found [24] as reported by Meng *et al*. [24] the calculated formation energies indicate that the substitution of a lattice titanium with an alkali-earth metal atom is energetically favorable. The electronic structure suggests that metal dopants shift the valence bands to higher energy [24].

Jensen *et al.* [22] introduced the plane-wave-based pseudo potential density functional theory to describe the doping impact of sulphur (S) substituting for oxygen (O) in anatase TiO_2 [22]. Electronic structure investigation demonstrates that the doping with S could generously bring down the band gap of TiO_2 by the nearness of a pollution condition of S 3p on the upper edge of the valence band. Excitations from the polluting which influence the condition of S 3p to the conduction band might be in charge of the red movement of the assimilation edge observed in the S-doped TiO_2.

The band narrow opening and the red movement of the assimilation edge are found to increase as the sulphur fixation increase.

Wang *et al.* [23] reported that nitrogen doped anatase TiO_2 is concentrated on utilizing crossover density functional theory estimations [23]. It is demonstrated that under average test conditions nitrogen likes to substitute at a Ti-site and attach to a few neighboring oxygen particles, shaping nitrite or nitrate atoms. This abandons one Ti-opportunity and under-facilitated oxygen atoms that deliver a substantial electron density of states at the valence band edge, with restricted characters marginally reaching out into the immaculate TiO_2 band gap, because of an adjusted nearby electrostatic potential and orbital associations. They propose that this extensive electronic density of states at the valence band gap is in charge of the upgraded sub gap tail assimilation which is observed in N-doped anatase TiO_2 and subsequently the obvious light photocatalytic action [24].

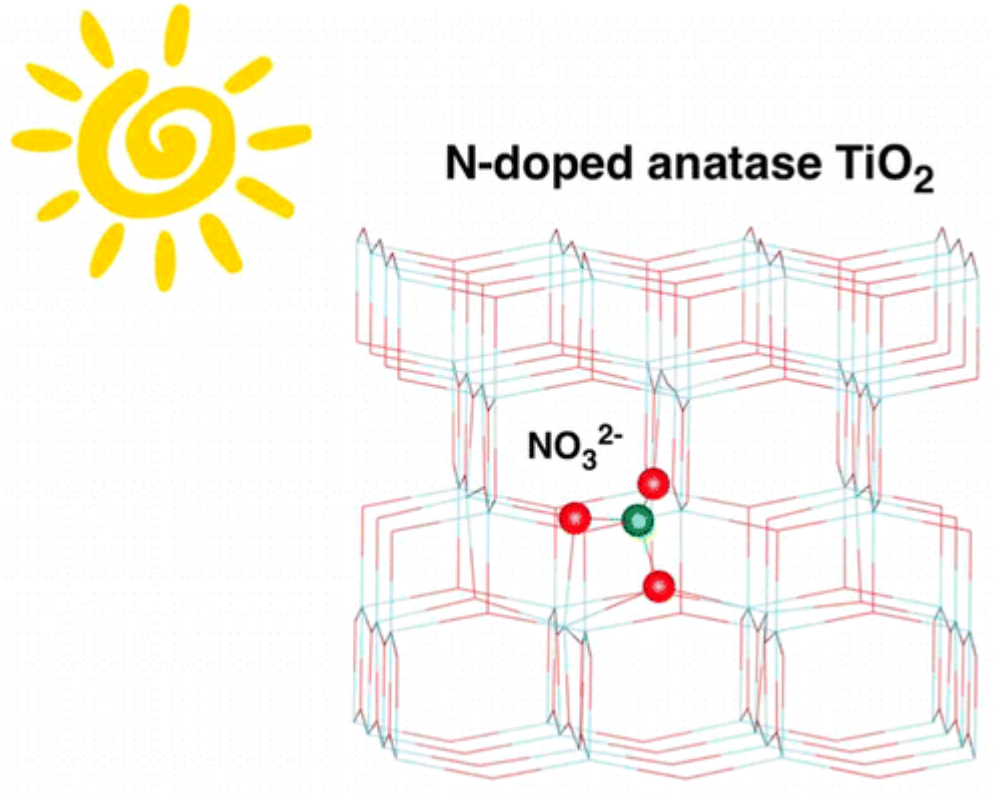

Figure 2.2: The N- doped anatase TiO_2 [24].

Wang *et al.* [7] reported the study on electronic structures of S-doped TiO_2 by first-principles computations in view of density functional theory with plane-wave ultrasoft pseudopotential strategy [7]. They discussed about anion doping and cations doping in anatase and rutile, they discovered diverse energy band structures and beginnings of photo activity of S-doped TiO_2. For anion-doped TiO_2, new S–3p groups show up and lie somewhat over the highest point of the O–2p valence band. It assumes a noteworthy part in expanding absorbance in the obvious locale, bringing about change in photocatalytic action under noticeable light illumination. For cations-doped TiO_2, the capability of the O–2p valence band move much downwards, yielding the more grounded oxidative force than that of undoped and S anion-doped TiO_2. The profound polluting influence states in band gap that begin from the S-dopant effect sly affect the recombination of the photo excited electrons [7].

2.3. The Dye Molecules

Typical DSSCs are composed of four major components: a wide band gap TiO_2 semiconductor, a dye-sensitizer to absorb photons from the sun, an electrolyte that creates the interface with the semiconductor and counter electrode carrying an electro-catalyst, which facilitates the transfer of electrons to the electrolyte. The dye molecule as sensitizer material, absorbs photon from the sun, become excited and inject an electron to the semiconductor, while the electrolyte regenerate the excited dye to complete the electron transport. [7, 25].

The organic dyes with visible light absorption usually possess a donor-p-acceptor configuration consisting of an electron donor and an electron acceptor, which are linked covalently through a p-conjugated bridge [26, 27]. Under light illumination, the photo-induced electrons transport through an intramolecular route in an organic dye are electron donor moiety, p-conjugated bridge, electron acceptor moiety, anchoring acid ligand, and finally enter the TiO_2 network, this charge transfer phenomenon is generally called the ‘electron injection’ which is the heart of solar to-electricity conversion processes in a DSSC [27]. In an organic dye, the tunable structure of the p-conjugated spacers is a key to influence both the highest occupied molecular orbital and the lowest unoccupied molecular orbital levels, and thereby the photo-physical properties of an organic dye [27]

The organic dyes with near-infrared light absorption are designed to improve the solar-to-electricity conversion efficiency by extending the absorption threshold of the organic dyes to the near infrared regions, which accounts approximately 45% of the total solar energy. Several near-infrared light absorption type organic dyes have been proposed for DSSCs. Chitumalla *et al.* [26] Investigated the excited-state properties of the croconate dyes with an aim to utilize them as light harvesting assemblies in the infrared (IR) region [26]. The excited singlet of the monomeric dye quickly deactivates without undergoing intersystem crossing to generate triplet. The triplet excited-state produced via triplet–triplet energy transfer method show relatively long life. The dye molecules when deposited as thin film on optically transparent electrodes or on nanostructured TiO_2 film form H-aggregates with a blue-shifted absorption maximum around 660 nm. The excitons formed upon excitation of the dye aggregates undergo charge separation at the TiO_2 and SnO_2 interface. The H-aggregates in the film are photoactive and produce anodic current when employed in a photo electrochemical cell. Spectroscopic and photo electrochemical experiments highlight the usefulness of croconate dyes in IR light harvesting applications [28]. Their results also shows that the highest occupied molecular orbitals (HOMOs) of the two dyes are situated mainly on the diketo groups, and partly on both the central croconate ring and the substituents. The lowest unoccupied molecular orbitals (LUMOs), however, are situated mainly on the central croconate ring and partly on the diketo groups and substituents [30]. In this study the focus is on the metal-free dyes called croconate dye, metal-free dyes have been intensively investigated to replace metal-based dyes. They include push-pull dyes, indolines, cumarines and polymethine dyes (squarylium, cyanine and croconate dyes) [29]. In general, especially with respect to ruthenium complexes, they show narrower, but more intense absorption bands. For this reason it is quite difficult to find a real panchromatic metal-free dye, while NIR absorbing dyes can be easily found in the class of polymethine dyes [29, 30].

Marcano E [31] explored, the absorption spectra, excited states and electronic injection parameters of anthocyanidin and anthocyanin pigments using the level of theory (TD) CAM-B3LYP/6-31+G(d,p). For the most isolated dyes, the distribution pattern of HOMO and LUMO spreads over the whole molecules, which lead an efficient electronic delocalization. The calculated light harvesting efficiencies (LHEs) are all near unity. Methoxy group in peonidin molecule lead the largest oscillator

strength and LHE. They illustrated that presence of water lead a higher spontaneous electronic inject process, with ΔG_{inject} average of –1.14 eV. The ΔG_{inject} order is peonidin < delphinidin < cyanin < cyanidin. Similarly, the adsorption energies (E_{ads}) onto anatase surface model were obtained from level of theory GGA(PBE)/DNP. E_{ads} of anthocyanin–$(TiO_2)_{30}$ complex was calculated to be from 17 to 24 eV, indicating both, the strong interactions between the dyes and the anatase (TiO_2) surface and stronger electronic coupling strengths of the anthocyanin–$(TiO_2)_{30}$ complex, which corresponded to higher observed η. The HOMO and LUMO shape showed the electrons delocalized predominantly on the anthocyanin structure while the LUMO + 1 shape is localized into the $(TiO_2)_{30}$ surface. Therefore, it was observed that there is electronic injection from HOMO to LUMO + 1 in the anthocyanin–$(TiO_2)30$ adsorption complex, after the light absorption [31].

Croconate dyes are another class of dye that exhibits absorption in the NIR region with a strong solvatochromic effect. The advantages over squaraine dyes are their stronger absorption, greater photostability and better yield [30]. However, this class of dye is still under investigation for DSSCs. Croconate dyes, CR-1, absorbs the light at 865 nm with a maximum IPCE around 1.2% at 650 nm. This croconate dyes does not show improved behavior with respect to other classes of dyes due to the net charge separation which is poor [26]. Besides, the overall photocurrent conversion efficiency remains rather low. During adsorption of croconate dye onto TiO_2 aggregation is a typical drawback which has to be solved before implementation in DSSCs [26].

2.4. Adsorption of Dye

Adsorption is defined as a process by which a material is concentrated on a solid surface from its liquid or gaseous surroundings. It involves trapping atoms or molecules that are incident on the surface. The adsorbate is the substance in the adsorbed state and the substance to be adsorbed is the adsorpt or adsorptive. The material onto which adsorption takes place is called the adsorbent [32].

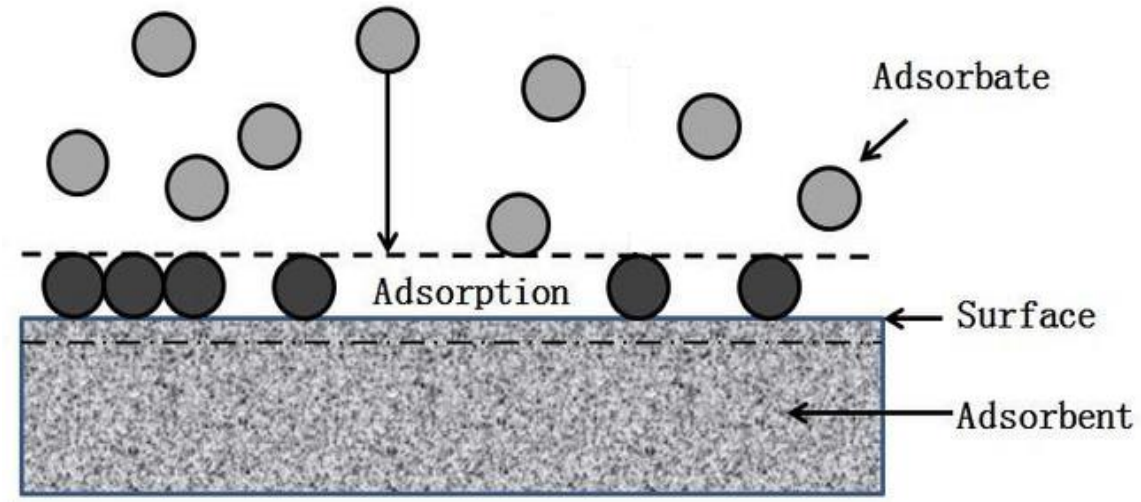

Figure 2.3: Basic terms of adsorption [32]

A distinction is drawn between adsorption and absorption. Adsorption is a surface based process while absorption is defined as transfer of a substance from one bulk phase to another bulk phase [34]. Given the need to better understand the behavior of the dyes adsorbed on the TiO_2 nanoparticle, Oprea *et al.* [34] investigated various single and double deprotonated forms of the dye bound to a TiO_2 cluster, taking advantage of the presence of the carboxyl, hydroxyl, and sulfonic groups as possible anchors. They reported that anchoring modes of the dye onto the TiO_2 surface are of crucial importance to the DSSC performance through the bonding type and the extent of electronic coupling between the dye excited state and the conduction band edge of the semiconductor [32].

As most of the theoretical studies so far have focused on sensitizers with carboxyl groups as anchors, they took advantage of the opportunity offered by the protonated form of the Mordant Yellow 10 dye, which has a –OH, $–CO_2H$ and $–SO_3H$ groups, to perform a comparative study of the various anchors, binding configurations as well as propensity for electron transfer [33]. They also studied the dye in various single and double deprotonated forms both free and anchored to a TiO_2 nanocluster in various binding configurations. First, they determined the proton affinity to identify the way the dye would tend to deprotonate, and further more they studied the distribution of charge on the dye for the key MOs to analyze the intramolecular charge transfer, following a push-pull approach. They also determined the distribution of charge on the anchoring

oxygen atoms to get an indication of the likelihood of the transfer to the substrate [34]. After optimizing the $Ti_{24}O_{50}H_4$ nanocluster, they studied the interacting dye-substrate system. The geometry optimization showed that the carboxyl group tends to bind in bidentate bridging configurations. The salycilate uses both the carboxyl and hydroxyl substituent groups to for either a tridentate binding to adjacent Ti(IV) ions or a bidentate Ti-O binding together with a O–H–O binding, due to the rotation out of the plane of the dye of the carboxyl group. The H-bonds strengthen mechanically the anchoring to the substrate when other binding pathways exist. However, in the absence of π binding pathways, the presence of an intermediate H atom can harm the charge injection. It is the presence of conjugated bonds, allowing for π electron delocalization, that facilitates the electron transfer.

To better understand the electron transfer process, they studied the distribution of charge on the cluster, on the entire sensitizer as well as on the various parts of the dye, and on the peripheral oxygen atoms. Their discussion was focused on the orbital overlap between the $\pi*$ orbital of the dye and the d orbitals of Ti (IV) ion. They reported that oxygen of the hydroxyl group offers in the context of a salicylate, a good electron transfer pathway, as it preserves the $\pi*$ nature of the dye MO. In contrast, in the case of the anchoring through the sulfonic group, the p orbitals of the oxygen atoms are moved away from the plane of the dye, to insure the proper binding to the neighboring metal ions, affecting the electron transfer pathway [31].

On the other work Oprea *et al.* [34] reported their results of density functional theory (DFT) and time-dependent DFT (TD-DFT) studies of several coumarin-based dyes, as well as complex systems consisting of the dye bound to a TiO_2 cluster. They provide the electronic structure and simulated UV-Vis spectra of the dyes alone and the dyes adsorbed to the cluster and discuss the matching with the solar spectrum. Furthermore they display the energy level diagrams and the electron density of the key molecular orbitals and analyze the electron transfer from the dye to the oxide. Finally, they compare the theoretical results with the experimental data available and discuss the key issues that influence the device performance [32].

The absorption spectra, which influence the light harvesting properties of the dyes, the energy level alignment between the dye, the oxide and the electrolyte, which affect the electron injection and the dye regeneration and the adsorption of the dye to the substrate and determination of the charge transfer was reported [33].The simulated UV-Vis absorption peaks of all coumarin dyes were found to be in good agreement with the experimental data. Due to the better matching of the solar irradiance spectrum, they concluded that NKX-2311 has superior light harvesting properties to both NKX-2398 and (especially to) C343. The analysis of the energy level alignment showed that for all free dyes, the LUMO lies above the conduction band edge of TiO_2, making possible the electron injection into the semiconducting oxide. In addition, the HOMO of all dyes lies well below the redox level of the electrolyte, allowing for the transfer of the electron to the dye and its regeneration. They commented on the inverse relation between the short-circuit current density and the energy difference between the excited state of the dye and the conduction band edge of the oxide, which is considered the driving force for the electron transfer. Based on the experimental values available, the also showed that, in the case of the dyes studied here, the short circuit current densities, Jsc, of the devices are negatively correlated with the driving force, as the short circuit current density is influenced not just by the energy difference between the excited state of the dye and the conduction band edge, but by other factors as well, such as the light harvesting efficiency and the propensity for electron transfer, not to mention recombination and leakage currents in the device [35]. They also discuss the charge transfer of the photoelectron from the excited state of the dye to the semiconductor based on an analysis of the electron density distribution over the ground and excited states of the dye [34, 35].

Using density functional theory (DFT) Niu *et al.* [36] investigated the structural and electronic properties of dye-sensitized solar cells (DSSCs) comprised of I-doped anatase TiO_2(101) surface sensitized with NKX-2554 dye, Their results indicate that the cyanoacrylic acid anchoring group in NKX-2554 has a strong binding to the TiO_2(101) surface.The dissociative and bidentate bridging type was found to be the most favorable adsorption configuration. On the other hand, the incorporations of I dopant can reduce the band gap of TiO_2 photoanode and improve the of NKX-2554 dye, which can improve the visible-light absorption of anatase TiO_2 and can also facilitate the electron injection from the dye molecule to the TiO_2 substrate. As a result,

the I doping can significantly enhance the incident photon-tocurrent conversion efficiency (IPCE) of DSSCs.They also shows in their results that the Fermi level of I doped TiO_2(101) surface is pinned at 0.16 eV above the conduction band minimum (CBM) so that iodine is effectively acting as an n-type dopant in TiO_2, showing a typical n-type metallic characteristic. Therefore, it is suggested that the I-doping can improve the conductivity of anatase TiO_2 photoanode. In fact, the open-circuit voltage (Voc) of DSSCs is determined by the energy difference between the CBM of TiO_2 electrode and the reduction level of hole-transport material (HTM). The n-type I-doping lead to the increase of the electron concentration and upward shift of the CBM, as a result, the Voc of of DSSCs is enlarged. These results are consistent with the corresponding experimental findings [36].

Moreover, It is also found that the I-doping in anatase TiO_2 (101) surface can facilitate the electron injection from the NKX-2554 dye to the TiO_2 substrate by analyzing the calculated electronic properties of adsorbed dye/TiO_2 complexes. Therefore, it is concluded that I doping can significantly enhance the IPCE of DSSCs due to the improved conductivity, increased open-circuit voltage, extended photo-response range of TiO_2 photoannode, and the effective electron injection of adsorbed dye/TiO_2 complexes [36].

Triggiani *et al.* [25] repoted that the adsorption of a tertiary amine (trimethylamine,TMA): on the three most exposed surfaces of anatase TiO_2 nanorods, i.e., (100), (001) and (101) using a periodic DFT and DFT-D. Their finding shows evidence of the formation of a coordinative bond between the molecules and the titanium site of adsorption. As per their expectation, the inclusion of dispersion correction strongly enhances the adsorption process. Moreover, in some cases TMA adsorption introduces new electronic states at the edge of the valence band. Overall, their results provide new insights on the interactions between TiO_2 nanorods and nitrogen compounds, which have many scientific and technological implications [25].

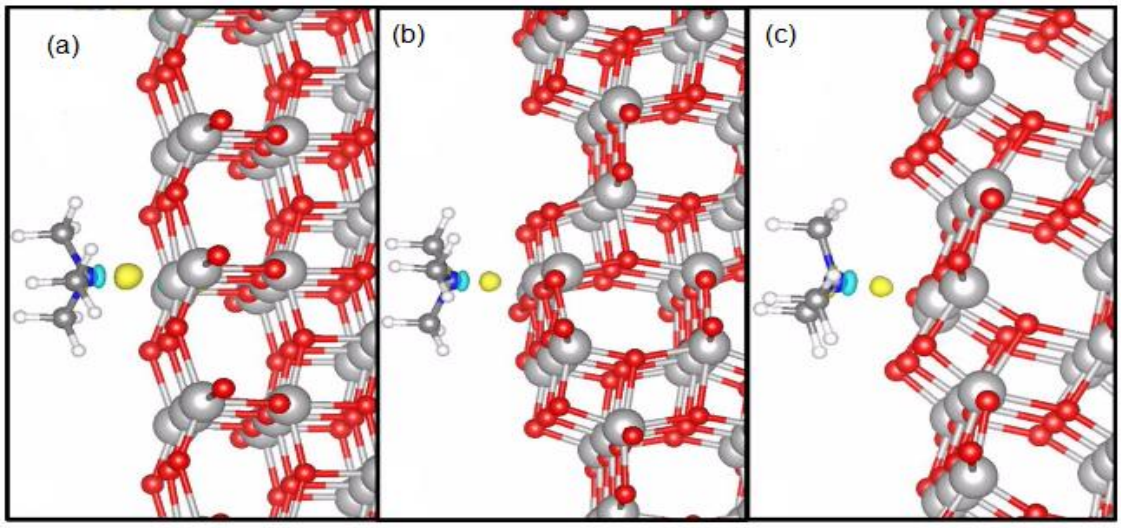

Figure 2.4: Three surfaces of anatase after adsorption of a TMA molecule. Image (a) refer to the anatase (001), Image (b) refer to the anatase (100) and Image (c) refer to the anatase (101) surfaces. Atom color code: red is oxygen, gray is titanium, blue is nitrogen, dark gray is carbon, white is hydrogen. Yellow and cyan areas indicate an increase and a decrease in electronic charge density after adsorption, respectively [37].

The adsorption of model croconate dyes on the TiO_2 anatase (101) surface has been studied by Puyad *et al.* [37] using the periodic density functional calculations to understand the adsorption of the diketo (-COCO-) groups. Their experimental and theoretical results have shown the strong binding ability of the acid group (-COOH) to the TiO_2 surface but the theoretical studies predicts the binding strength of the diketo group to be also significant and comparable with that of the -COOH group. This causes a competitive binding between the diketo groups and the acid groups on the TiO_2 surface in the case of croconate dyes and cause a reduction in the efficiency of the DSSC. They also reported that binding energy obtained clearly points out to large values of around 23.2 to 28.7 kcal/mol depending on the donor groups on the croconate ring. The molecule with larger biradical character also has a smaller binding energy. Thus, their study shows that the binding of the keto groups of the croconate dyes are competitive with the carboxylic acid groups [37].

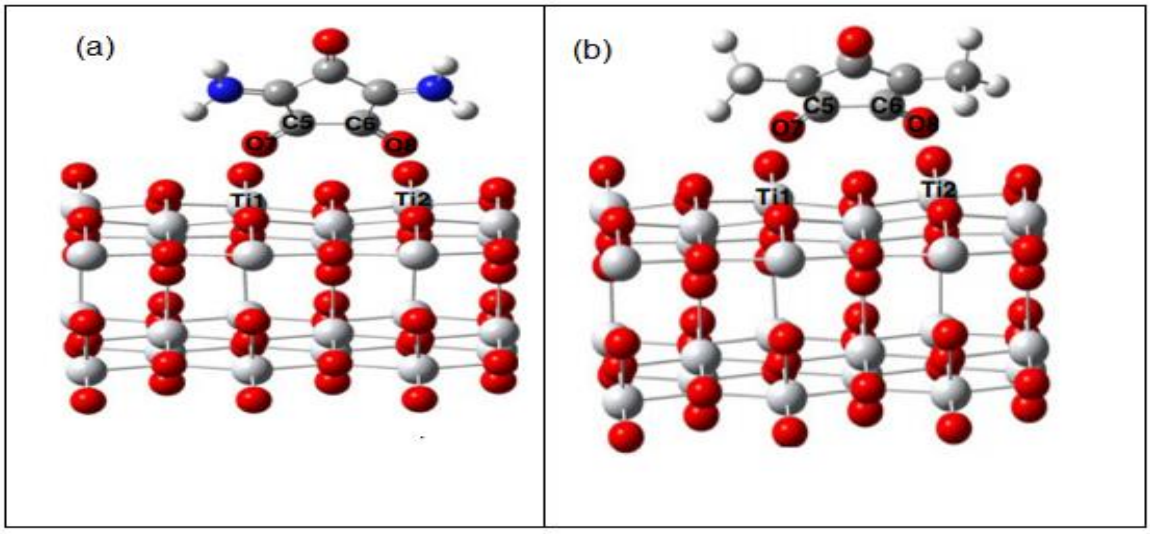

Figure 2.5: The Adsorption of diketo group of Croconate dyes in bidentate bridging (BB) fashion. Image (a) Adsorption of diketo group of (-COCO-) on the TiO_2 anatase (101) and Image (b) Adsorption of acid group of (-COOH-) on the TiO_2 anatase (101) [26]

Chitumalla *et al.* [26] investigated the two models of croconate dyes, one with an electron-donating substituent (CR1) and the other with an electron-withdrawing group (CR2) using the density functional theory (DFT). The geometric, electronic, and optical properties of these dyes were compared. Upon switching from CR1 to CR2, a considerable bathochromic shift was observed in the electronic absorption spectrum. They also investigated the adsorption behaviour of the two dyes on a TiO_2 (101) anatase surface by employing periodic DFT simulations. The periodic electronic-structure calculations revealed that the diketo group of CR1 bound more strongly to the TiO_2 surface than that of CR2, with a binding strength comparable to that of a typical organic D–π–A dye [26]. They further illustrate that the obtained binding energy points out to large values of around 23.2 to 28.7 kcal/mol clearly depending on the donor groups on the croconate ring. The molecule with larger biradical character also has a smaller binding energy. Thus their study shows that the binding of the keto groups of the croconate dyes are competitive with the carboxylic acid groups [26].

3. CHAPTER 3 METHODOLOGY

3.1. Density Functional Theory

Density functional theory (DFT) is a computational quantum mechanical method used in physics, chemistry and materials science to examine the electronic structure (principally the ground state) of numerous systems, in particular atoms, molecules and the dense stages [40].DFT calculations are based on solving Kohn–Sham equation, which is the Schrödinger equation of an invented system of non-associating particles that produce an indistinguishable density from any given arrangement of connected particles [38,39]. The Kohn–Sham equation is characterized by a nearby viable outside potential in which the non-cooperating particles move, commonly meant as $V_s(r)$ or $V_{eff}(r)$, called the Kohn–Sham potential. As the particles in the Kohn–Sham equation are non-collaborating fermions, the Kohn–Sham wavefunction is a solitary slater determinant developed from an arrangement of orbitals that are the most minimal energy. The wave function equation is then given by [38]:

$$\left(-\frac{\hbar^2}{2m}\nabla^2 + v_{eff}(\mathrm{r})\right)\phi_i(\mathrm{r}) = \varepsilon_i\phi_i(\mathrm{r}) \qquad (1)$$

This eigenvalue equation is the typical representation of the Kohn–Sham equations. where, ε_i is the orbital energy of the corresponding Kohn–Sham orbital, φ_i, and the density for an N-particle system is given by [40]:

$$\rho(\mathrm{r}) = \sum_{i}^{N}\left|\phi_i(\mathrm{r})\right|^2 \qquad (2)$$

In Kohn-Sham density functional theory, the aggregate energy of the system is described as a useful charge density given as:

$$E[\rho] = T_s[\rho] + \int drV_{ext}(r)\rho(r) + E_H[\rho] + E_{xc}[\rho] \qquad (3)$$

where T_s is the Kohn–Sham kinetic energy described as the Kohn–Sham orbitals and is given by:

$$T_s[\rho] = \sum_{i=1}^{N} \int dr \phi_i^*(r) \left(-\frac{\hbar^2}{2m} \nabla^2 \right) \phi_i(r) \tag{4}$$

V_{ext} is the outside potential following up on the cooperating system (at least, for an atomic system, the electron-cores), E_H is the Hartree energy given as:

$$E_H = \frac{e^2}{2} \int dr \int dr' \frac{\rho(r)\rho(r')}{|r - r'|} \tag{5}$$

and E_{xc} is the exchange-correlation energy. The Kohn–Sham equations are found by varying the total energy expression with respect to a set of orbitals to yield the Kohn–Sham potential as [33]:

$$V_{eff}(r) = V_{ext}(r) + e^2 \int \frac{\rho(r')}{|r - r'|} dr' + \frac{\delta E_{xc}[\rho]}{\delta \rho(r)} \tag{6}$$

where the last term is depicted by:

$$v_{xc}(r) \equiv \frac{\delta E_{xc}[\rho]}{\delta \rho(r)} \tag{7}$$

is the exchange-correlation potential. These terms and the corresponding energy expression, are the only unknowns in the Kohn–Sham approach to density functional theory. An approximation that does not vary the orbitals is Harris functional theory [41].

The Kohn–Sham orbital energies ε_i, in general, have little physical meaning. The sum of the orbital energies is related to the total energy by:

$$E = \sum_{i}^{N} \varepsilon_i - V_H[\rho] + E_{xc}[p] - \int \frac{\delta E_{xc}[\rho]}{\delta \rho(r)} \rho(r) dr \tag{8}$$

Because the orbital energies are non-unique in the more general restricted open-shell case, this equation only holds true for specific choices of orbital energies. Since the orbital energies are non-one of a kind in the broader limited open-shell case, this condition remains constant for particular decisions of orbital energies [42, 43].

The modern DFT is founded on Hohenberg–Kohn theorems and the two theorems relate to any system consisting of electrons moving under the influence of an external potential.

Theorem 1. The external potential (and hence the total energy), is a unique functional of the electron density.

If two systems of electrons, one trapped in a potential $V_1(\vec{r})$ and the other in $V_2(\vec{r})$ have the same ground-state density $n(\vec{r})$, then $V_1(\vec{r}) - V_2(\vec{r})$ is necessarily a constant.

Corollary: The ground state density uniquely determines the potential and thus all properties of the system, including the many-body wave function. In particular, the $H - K$ functional, defined as $F[n] = T[n] + U[n]$, is a universal functional of the density (not depending explicitly on the external potential).

Theorem 2. The functional that delivers the ground state energy of the system, gives the lowest energy if and only if the input density is the true ground state density.

For any positive integer n and potential $V(\vec{r})$,a density functional F[n] exists such that:

$$E_{(v,N)}[n] = F[N] + \int v(\vec{r})n(\vec{r})d^3r \qquad (9)$$

The density functional obtains its minimal value at the ground-state density of N electrons in the potential$(\vec{r})$. The minimal value of $E_{(v, N)}$ [n] is then the ground state energy of this system [44].

The major problem with DFT is that the exact functionals for exchange and correlation are not known except for the free electron gas. However, approximations exist which permit the calculation of certain physical quantities quite accurately [45]. In physics the most widely used approximation is the local-density approximation (LDA).

3.2. Local Density Approximations

Local density approximation (LDA) is a class of approximations to the exchange–correlation (XC) energy functional in density functional theory. It depends exclusively upon the estimation of the electronic density at every point in space. Numerous methodologies can yield local approximations to the XC energy. Overwhelmingly effective nearby approximations can be also defined as those that have been established from the homogeneous electron gas (HEG). In such manner, LDA is for the most part synonymous with functional in light of the HEG estimate, which are then connected to practical frameworks.

For a spin-unpolarized framework, a local density approximation for the exchange correlation energy is expressed as [46, 47]:

$$E_{xc}^{LDA}[\rho] = \int \rho(r)\varepsilon_{xc}(\rho)\,\mathrm{dr} \tag{10}$$

where ρ is the electronic density, ε_{xc} is the exchange-correlation energy per molecule of a homogeneous electron gas of charge density. The exchange-correlation energy is decayed into exchange and correlation terms linearly and can be expressed as [50]:

$$E_{xc} = E_x + E_c \tag{11}$$

so that different expressions for E_x and E_c are looked for. The exchange term goes up against a straightforward systematic frame for the HEG. Just restricting expressions for the relationship thickness are known precisely, prompting various distinctive approximations for E_c.

Local density approximations are imperative in the development of more complex approximations to the exchange-correlation energy, for example, generalized gradient approximations or hybrid functionals, as an attractive property of any exchange-correlation functional, is that, it duplicates the correct consequences of the HEG for non-differing densities. In that capacity, LDA's are frequently an express segment of such functionals [46].

The LDA assumes that the density is the same everywhere. Because of this, the LDA has a tendency to underestimate the exchange energy and over-estimate the

correlation energy. The errors due to the exchange and correlation parts tend to compensate each other to a certain degree. To correct for this tendency, it is common to expand in terms of the gradient of the density in order to account for the non-homogeneity of the true electron density. This allows for corrections based on the changes in density away from the coordinate. These expansions are referred to as Generalized Gradient Approximation (GGA) [46].

3.3. Generalized Gradient Approximation

As the LDA approximates the energy of the genuine density by the energy of a local constant density, it falls flat in circumstances where the thickness experiences quick changes, for example, in atoms. A change to this can be made by considering the slope of the electron density, the alleged GGA. The LDA exchange-correlation is an inhomogeneous system in non-local density as for electrons it encompasses, and this is alluded to as inclination amendment or realized gradient approximation GGA. The GGA exchange-correlation energy is given as [46, 47]:

$$\mathrm{E_x^{GGA}c(n)} = \int \mathrm{dn(r)\varepsilon_{xc}^{GGA}[n(r), \| \nabla n(r) \|]} \quad (15)$$

where $\mathcal{E}_{xc}$ is the exchange correlation energy and $n(r)$ is the gradient term. The GGA has been broadly utilized and have turned out to be very fruitful in remedying a portion of the inadequacies of the LDA [48].

3.4. Planewave Pseudopotential Method

3.4.1. Planewave Basis

Plane-wave basis sets is used in quantum-chemical simulations. Typically, the choice of the plane wave basis set is based on a cutoff energy. The plane waves in the simulation cell fit below the energy criterion and are then included in the calculation [49]. These basis sets are popular in calculations involving three-dimensional periodic boundary conditions.

The main advantage of a plane-wave basis is that it is guaranteed to converge in a smooth, monotonic manner to the target wavefunction. In contrast, when localized basis sets are used, monotonic convergence to the basis set limit may be difficult due to problems with over-completeness: in a large basis set, functions on different atoms start to look alike, and many eigenvalues of the overlap matrix approach zero [50].

In addition, certain integrals and operations are much easier to program and carry out with plane-wave basis functions than with their localized counterparts. For example, the kinetic energy operator is diagonal in the reciprocal space. Integrals over real-space operators can be efficiently carried out using fast Fourier transforms. The properties of the Fourier Transform allow a vector representing the gradient of the total energy with respect to the plane-wave coefficients to be calculated with a computational effort that scales as NPW*ln(NPW) where NPW is the number of plane-waves. When this property is combined with separable pseudo potentials of the Kleinman-Bylander type and pre-conditioned conjugate gradient solution techniques, the dynamic simulation of periodic problems containing hundreds of atoms becomes possible [49,50].

In practice, plane-wave basis sets are often used in combination with an 'effective core potential' or pseudopotential, so that the plane waves are only used to describe the valence charge density. This is because core electrons tend to be concentrated very close to the atomic nuclei, resulting in large wavefunction and density gradients near the nuclei which are not easily described by a plane-wave basis set unless a very high energy cut-off, and therefore small wavelength, is used. This combined method of a plane-wave basis set with a core pseudo potential is often abbreviated as a PSPW calculation [51].

Furthermore, as all functions in the basis are mutually orthogonal and are not associated with any particular atom, plane-wave basis sets do not exhibit basis-set superposition error. However, the plane-wave basis set is dependent on the size of the simulation cell, complicating cell size optimization [50].

Due to the assumption of periodic boundary conditions, plane-wave basis sets are less well suited to gas-phase calculations than localized basis sets. Large regions of vacuum need to be added on all sides of the gas-phase molecule in order to avoid interactions with the molecule and its periodic copies. However, the plane waves use

a similar accuracy to describe the vacuum region as the region where the molecule is, meaning that obtaining the truly noninteracting limit may be computationally costly [51].

3.4.2. Pseudopotential Method

A pseudopotential or effective potential is used as an approximation for the simplified description of complex systems. Applications include atomic physics and neutron scattering. The pseudopotential approximation was first introduced by Hans Hellmann in 1934 [52].

The pseudopotential is an attempt to replace the complicated effects of the motion of the core electrons of an atom and its nucleus with an effective potential, or pseudopotential, so that the Schrödinger equation contains a modified effective potential term instead of the Coulombic potential term for core electrons normally found in the Schrödinger equation.

The pseudopotential is an effective potential constructed to replace the atomic all-electron potential such that core states are eliminated and the valence electrons are described by pseudo-wavefunctions with significantly fewer nodes [53]. This allows the pseudo-wavefunctions to be described with far fewer Fourier modes, thus making plane-wave basis sets practical to use. In this approach usually only the chemically active valence electrons are dealt with explicitly, while the core electrons are being considered together with the nuclei as rigid non-polarizable ion cores. It is possible to self-consistently update the pseudopotential with the chemical environment that it is embedded in, having the effect of relaxing the frozen core approximation, although this is rarely done. In codes using local basis functions, like Gaussian, often effective core potentials are used that only freeze the core electrons.

First-principles pseudopotentials are derived from an atomic reference state, requiring that the pseudo- and all-electron valence eigenstates have the same energies and amplitude (and thus density) outside a chosen core cut-off radius.Pseudopotentials with larger cut-off radius are said to be softer, that is more rapidly convergent, but at the same time less transferable, that is less accurate to reproduce realistic features in different environments [54].

Early applications of pseudopotentials to atoms and solids based on attempts to fit atomic spectra achieved only limited success. Solid-state pseudopotentials achieved their present popularity largely because of the successful fits by Walter Harrison to the nearly free electron Fermi surface of aluminum (1958) and by James C. Phillips to the covalent energy gaps of silicon and germanium (1958). Phillips and coworkers (notably Marvin L. Cohen and coworkers) later extended this work to many other semiconductors, in what they called "semi empirical pseudopotentials" [55].

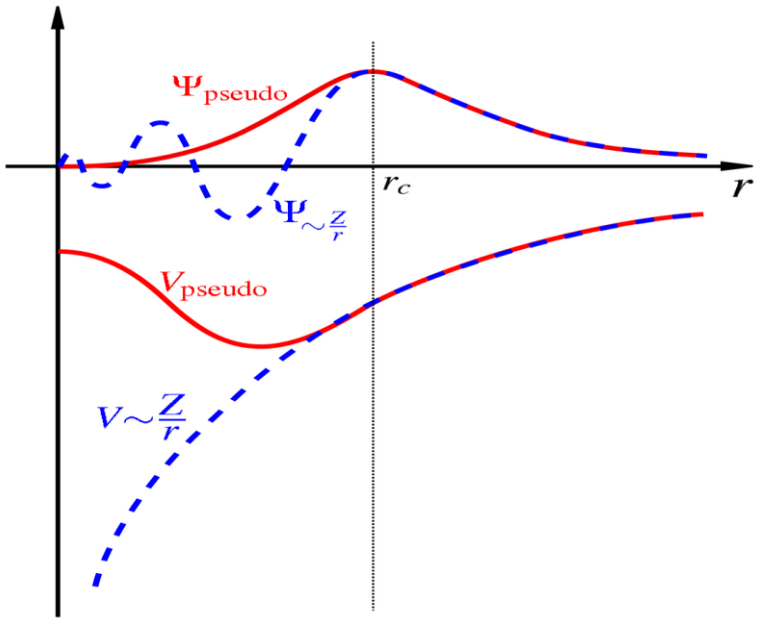

Figure 3.1: Comparison of a wave function in the Coulomb potential of the nucleus (blue) to the one in the pseudopotential (red). The real and the pseudo wave function and potentials match above a certain cut-off radius c_r

3.4.3. Norm-Conserving Pseudopotential

Norm-conserving and ultrasoft are the two most common forms of pseudopotential used in modern plane-wave electronic structure calculations. They allow a basis-set with a significantly lower cut-off (the frequency of the highest Fourier mode) to be used

to describe the electron wave functions and so allow proper numerical convergence with reasonable computing resources. An alternative would be to augment the basis set around nuclei with atomic-like functions, as is done in Linearized Augmented Planewave (LAPW). Norm-conserving pseudopotential was first proposed by Hamann, Schlüter, and Chiang (HSC) in 1979 [56]. The original HSC norm-conserving pseudopotential takes the following form:

$$\hat{V}_{ps}(r) = \sum_i \sum_m |Y_{im}\rangle\, V_{im}(r) \langle Y_{im}| \tag{16}$$

where $Y_{im}\rangle$ projects a one-particle wave function, such as one Kohn-Sham orbital, to the angular momentum labeled by $\{l, m\}$. $V_{im}(r)$ is the pseudopotential that acts on the projected component. Different angular momentum states then feel different potentials, thus the HSC norm-conserving pseudopotential is non-local, in contrast to local pseudopotential which acts on all one-particle wave-functions in the same way.

Norm-conserving pseudopotentials are constructed to enforce two conditions.

1. Inside the cut-off radius r_c the norm of each pseudo-wave function be identical to its corresponding all-electron wave function [57]:

$$\int_{r_c}^{r} dr^3 \emptyset_{R,i}(\vec{r}) \emptyset_{R,j}(\vec{r}) = \int_{r_c}^{r} dr^3 \tilde{\emptyset}_{R,i}(\vec{r})\, \tilde{\emptyset}_{R,j}(\vec{r}) \tag{17}$$

where $\emptyset_{R,i}$ and $\tilde{\emptyset}_{R,i}$ are the all-electron and pseudo reference states for the pseudopotential on atom R

3.4.4. Ultrasoft Pseudopotentials

Ultrasoft pseudopotentials relax the norm-conserving constraint to reduce the necessary basis-set size further at the expense of introducing a generalized eigenvalue problem with a non-zero difference in norms we can now define [51] :

$$qR_{,ij} = \langle \emptyset_{R,i} | \emptyset_{R,j} \rangle - \langle \tilde{\emptyset}_{R,i} | \tilde{\emptyset}_{R,j} \rangle \tag{18}$$

And so m=normalized eigenstate of the pseudo Hamilitonian now obeys the generalized equation

$$\hat{H}|\Psi_i\rangle = \epsilon_i \hat{S}|\Psi\rangle \tag{19}$$

Where the operator $\hat{S}$ is defined as

$$\hat{S} = 1 + \sum_{R,i,j} |PR, i\rangle QR, ij\langle PR, j| \quad (20)$$

where PR, i are projectors that form a dual basis with the pseudo reference states inside the cut-off radius, and are zero outside:

$$\langle PR, i|\tilde{\phi}_{R,j}\rangle_{r<r_c} = \delta_{i,j} \quad (21)$$

A related technique is the projector augmented wave (PAW) method [48].

3.5. Brilloun Zone

In mathematics and solid state physics, the first Brillouin zone is a uniquely defined primitive cell in reciprocal space. In the same way the Bravais lattice is divided up into Wigner–Seitz cells in the real lattice, the reciprocal lattice is broken up into Brillouin zones. The boundaries of this cell are given by planes related to points on the reciprocal lattice. The importance of the Brillouin zone stems from the Bloch wave description of waves in a periodic medium, in which it is found that the solutions can be completely characterized by their behavior in a single Brillouin zone [49].

The first Brillouin zone is the locus of points in reciprocal space that are closer to the origin of the reciprocal lattice than they are to any other reciprocal lattice points. Another definition is as the set of points in *k*-space that can be reached from the origin without crossing any Bragg plane. Equivalently, this is the Voronoi cell around the origin of the reciprocal lattice [50].

3.6. K-point sampling

For a periodic system, the K-points appearing in the wave function belong to the first Brillouin zone, by virtue of the Bloch's theorem. In the case of samples with defects, which are by definition aperiodic, the cell that contains the deffects is periodically repeated, using periodic boundaries. The Bloch theorem can therefore be applied to this supercell, the dimension of the Brillouin zone being determined by the dimension of the supercell itself, i. e. the larger the supercell, the smaller the Brillouin zone should be [51].

To calculate the energy band, or the charge density for example, the sum over these K-points has to be done. Therefore, choosing a sufficiently dense mesh of summation is crucial for the convergence of the results. Monkhorst and Pack [53, 54] proposed a scheme where the K-are distributed homogeneously in the Brillouin zone according to

$$K = x_1 b_1 + x_2 b_2 + x_3 b_3 \tag{22}$$

where b_1, b_2 , b_3 are the reciprocal lattice vectors, and

$$x_i = \frac{l}{n_i} \qquad l = 1, \dots, n_1 \tag{23}$$

where n_i are the folding parameters [51,52].

Usually, total energies of different structures are compared. Therefore, if the two structures have the same unit cell, the same set of K-points should be used. Since only the difference in the energies of the two structures is required, possible errors from a non-converged K-point sampling may cancel out. The computational effort could therefore be reduced by using a carefully chosen and small K-point set.

An alternative method for choosing **k**-point mesh has been proposed by Chadi and Cohen [65,66], on the basis of ``shells'' analysis. This concept can be explained by considering the Bloch function for a specific band as [53]:

$$\varphi_k(r) = \frac{1}{\sqrt{N}} \sum_{Rj} \exp(iK.R_i)\varphi(r - R_i) \tag{24}$$

The charge density for this specific state is therefore

$$p_k(r) = \frac{1}{N} \sum_{R_i R_j} exp\,[iK.(R_i - R_j)]\varphi^*(r - R_j)\varphi(r - R_i) \tag{25}$$

which can be rewritten as

$$p_k(r) = \frac{1}{N} \sum_{Ri} |\varphi(r - R_i)| + \frac{1}{N} \sum_{Ri} \sum_{Rj} \exp[iK.R_i]\varphi^{*\prime}(r + R_j + R_i)\varphi(r - R_i) \tag{26}$$

where the prime in the second sum is over all *l*, except the $R_i = 0$ term. Equation (26) should be compared to the total charge density, given by

$$p(r) = \sum_k pk(r) = \sum_{Ri} |\varphi(r - R_i)| \tag{27}$$

One can see that the first term in equation (26) is the average charge density for the band considered. It could therefore be a reliable approximation to the total charge density, providing a good choice of K-points are chosen that minimize the second term in equation (26) [52,53].

3.7. Computational Details

The structures of the dye molecules was built using Material Studio package. The dye molecules structures were cleaned so that the atoms are reoriented in their lattice positions. Geometrical optimization of the dye molecules was performed by CASTEP code in Material Studio package using density functional theory (DFT), CASTEP is a commercial programming bundle which utilizes density functional with a plane wave premise set to figure the electronic properties of crystalline solids, surfaces, atoms, fluids and formless materials from first standards. The plane-wave pseudopotential method, generalized gradient approximation (GGA) in the scheme of Perdew-Bruke-Ernzerhof (PBE) to describe the exchange-correlation functional and the cutoff energy for plane-wave basis set to 650 eV. 7 x 7 x 3 monkhorst-pack was used in DFT calculation with all band/ Ensemble density functional theory (EDFT) as electronic minimizer was used. All structure were inside the vacuum slab of 10.00 Å vacuum thickness, 17.552 Å and 0.00 Å slab position.

The ground state structures obtained through geometrical optimization was imported into a new 3D atomistic window and the optical absorption of dye molecules were calculated, then the calculations of electronic properties and UV-Vis of the ground state structures were done using VAMP module within the Material Studio package. VAMP is a semi-empirical molecular orbital package for molecular organic and inorganic systems, it is an ideal intermediate module between force-field and first principles methods and is capable of rapidly calculating many physical and chemical molecular properties.

Anatase TiO_2 bulk structures were also optimized using CASTEP code within the frame work of the Material Studio package to obtain the ground state properties of the anatase TiO_2 structure, GGA-PBE functional for geometrical optimization and

investigation of the convergence parameters of anatase TiO_2 structure were used, the fixed basis set and ultra-soft pseudopotential was used throughout the study. The ground state structures obtained through geometrical optimization with the convergence parameters were imported into a new 3D atomic window and the surfaces were cleaved from the bulk structure and a vacuum slab of appropriate size was built for the surface structures. After this process, the surfaces were optimized using the same convergence parameters obtained for the bulk structures. The dye/TiO_2 complex was optimized to obtain the ground state structures, and the electronic properties were calculated using CASTEP code.

4. CHAPTER 4 : Results and Discussion

4.1. Titanium Dioxide Semiconductor

4.1.1. Convergence Test

The convergence tests were performed in order to find a suitable energy cut-off and k-points to simulate the systems. Figure 4.1 shows the total energy against the cut-off energy diagram of anatase TiO_2 bulk structure. It was observed that from 650 eV the graph become stable suggesting that the energy has converged. The value of 650 eV was chosen as a cut-off energy which was used to compute all calculation throughout the study.

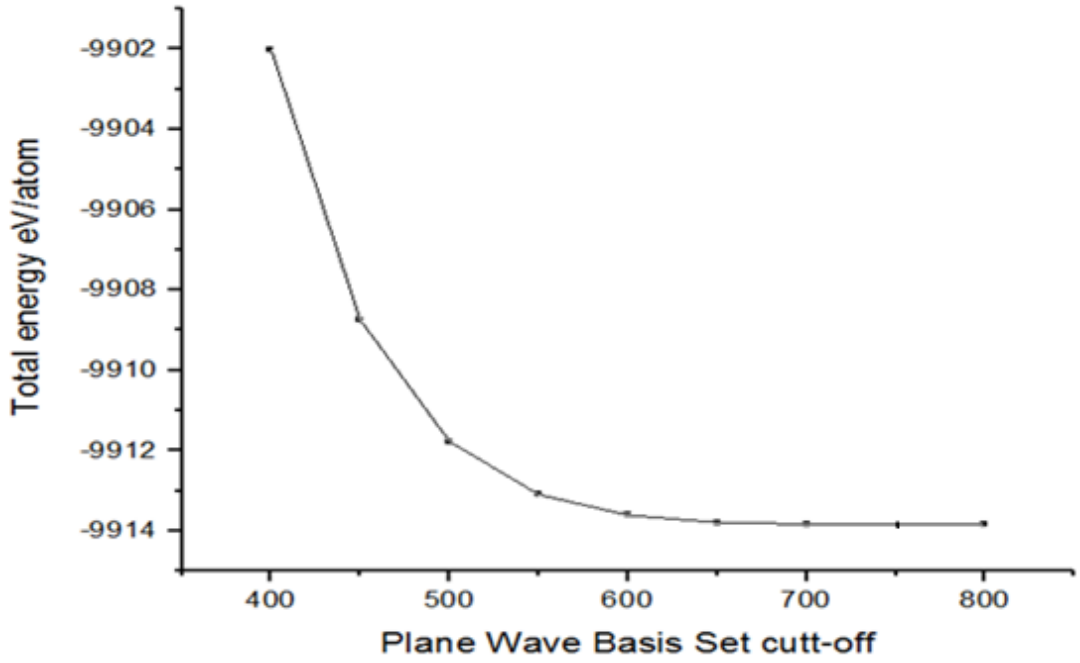

Figure 4.1: Total energy as a function of energy cut-off graph for pure anatase TiO_2.

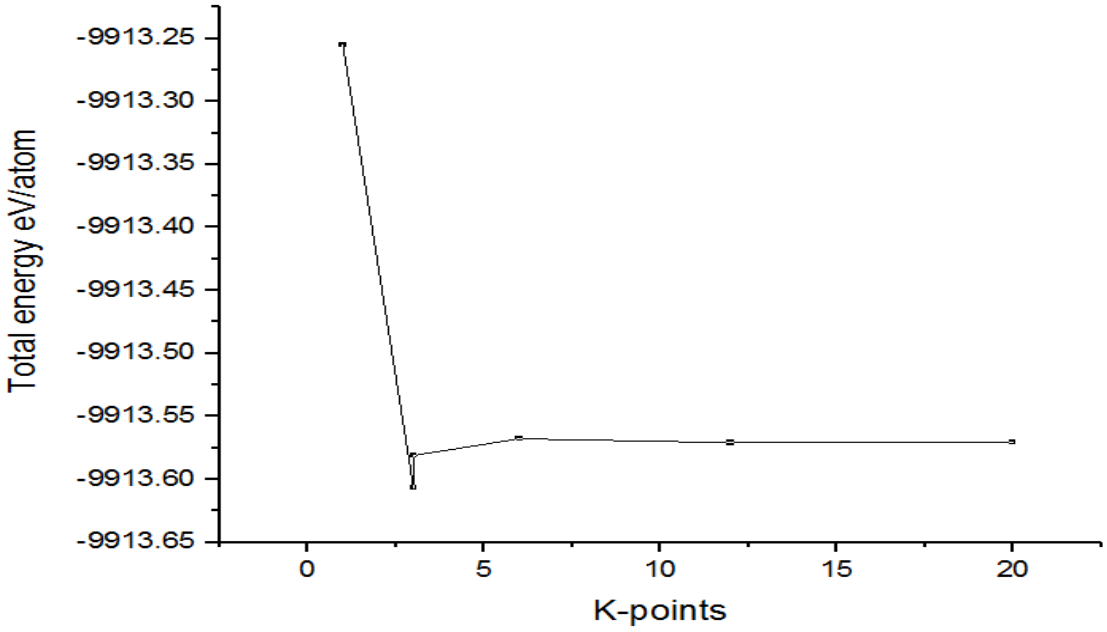

Figure 4.2: number of k-points used v/s final energy.

Figure 4.2 illustrates total energy of the system as a function of k-points and the calculated minimum total energy was found to be -9913.570 eV which corresponds to 7 x 7 x 3 k-mesh parameters and corresponding k-points were considered as the most preferred mesh.

4.1.2. Structural Properties

Anatase is a member of the TiO_2 polymorphs family together with rutile and brookite. In this study geometry optimization of the bulk structure of anatase TiO_2 was performed as a way of validating the model used in the study. The calculations were performed using a set of k-points and energy cut-off that were determined through the convergence test as discussed in the previous section. Geometry optimization calculations were performed in one steps with the unconstrained volume, to determine equilibrium bulk parameters and respective energies. Figure 4.3 shows the bulk structure of anatase TiO_2.

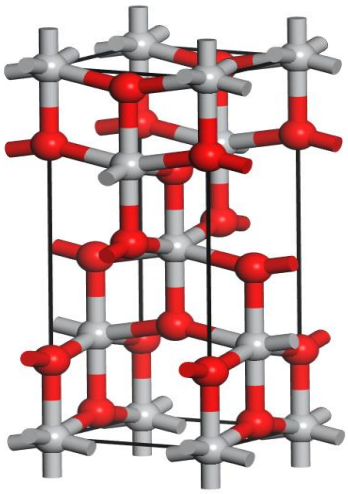

Figure 4.3: TiO_2 anatase bulk structure

The ground state energy structure for pure anatase TiO_2 was determined by calculating the lattice parameters with their corresponding lowest energy. Table 4.1 shows the calculated lattice parameters a, b and c, compared with the reported experimental values and previous theoretical results. It can be observed that calculated results are in good agreement with reported results from literature [53, 54]. The lattice parameters obtained in this work are comparable to the experimental data, with a deviation of 0.0088 % along a- and b-axes and 0.0264 % along the c-axis. The results gave a percentage error that is within reasonable and acceptable value as determined by various density functional theory methods [54].

Table 4.1: Optimized structural parameters for bulk anatase TiO_2 compared with experimental and previous theoretical results

Lattice Parameter	EXPERIMENTAL [53]	THIS WORK		LITERATURE [54]	
		Results	Deviation (%)	Results	Deviation (%)
a (Å)	3.785	3.776	0.0088	3.743	0.042
b (Å)	3.785	3.776	0.0088	3.743	0.042
c (Å)	9.512	9.486	0.0264	9.481	0.031

.

The optimized structural parameters show that the computed results obtained are in good agreement with the experimental and other theoretical reported values [54]. The calculated deviations from the experimental results are fair compared to those reported in the literature [53].

Figures 4.4 and 4.5 represent (010 and 100) anatase TiO_2 surfaces cleaved from anatase TiO_2 bulkstructure.The atoms in this surfaces are having some cleaved bonds in the termination position , while terminating with both oxygen and titanium. The surfaces were optimized by relaxing atoms to eliminate surface tension.

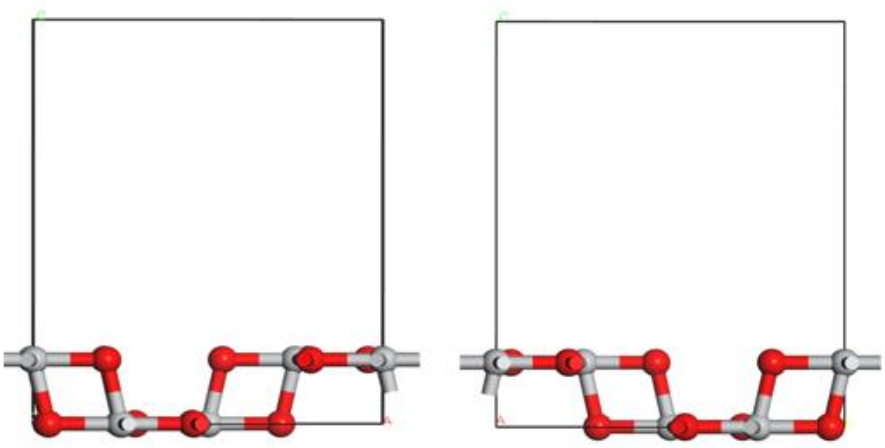

Figure 4.4: TiO_2 anatase (010) and (100) surfaces

4.1.3. Electronic Properties

4.1.3.1. Band Structure

There are two requirements for transitions of electrons between the valence and the conduction band and vice versa, i.e. both the energy and momentum have to be conserved. The conservation of energy usually is not a problem in direct and indirect semiconductors. For an electron transition between the maximum of the valence band and the minimum of the conduction band, or vice versa, the conservation of momentum, however, cannot be fulfilled with the absorption or emission of a photon alone in an indirect semiconductor, because the magnitude of the momentum of a photon is several orders of magnitude smaller than that of an electron in a semiconductor. The same large difference holds between the wave vectors of a photon and an electron in a crystal. It is therefore, possible to compare the momenta or the wave vectors. The energy bands in dependence on the wave vector are calculated from the Schrödinger equation with a periodic potential that is characteristic for certain semiconductors [58,59]. In addition to a photon, a phonon has to be absorbed or emitted in order to conserve the momentum. Phonons are quantized lattice vibrations. They possess small energies (up to approximately 100 meV) and a momentum of the order of that of an electron in a semiconductor. Many phonons are present in crystals like semiconductors at room temperature [60].

The band gap generally refers to the energy difference between the top of the valence band and the bottom of the conduction band in insulators and semiconductors. The calculated band gap of pure anatase TiO_2 is about 2.118 eV, which is smaller than the experimental value of 3.2 eV due to the underestimation of band gap by GGA functional employed the DFT. The calculated band gap of cleaved surface TiO_2 anatase (100) is 2.834 eV which is about 0.716 greater than the calculated band gap of pure anatase TiO_2, but it is 0.366 eV smaller than the experimental value. The calculated band gap of cleaved surface TiO_2 anatase (010) is 2.600 eV, which is 0.482 eV greater than the calculated band gap of pure anatase TiO_2, but 0.600 eV smaller than the experimental value. The calculated band gap of two surface structures are found to be greater than the band gap of bulk structure, this difference in the band gap

of bulk structure and surfaces is due to cleaving, when the structure is being cleaved the re-orientation of atoms occurs.

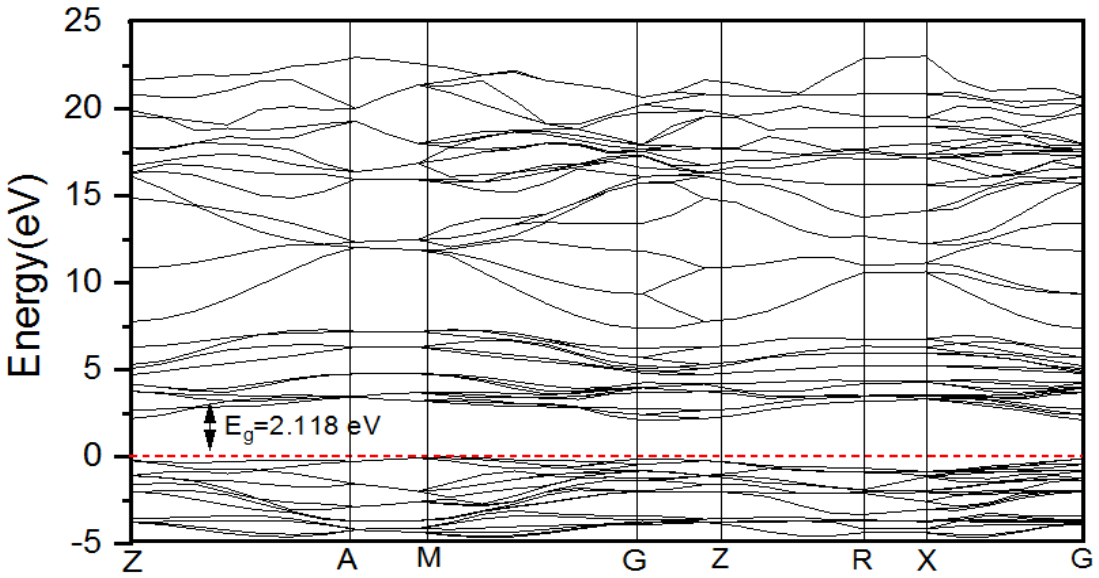

Figure 4.5: TiO_2 anatase bulk structure band structure

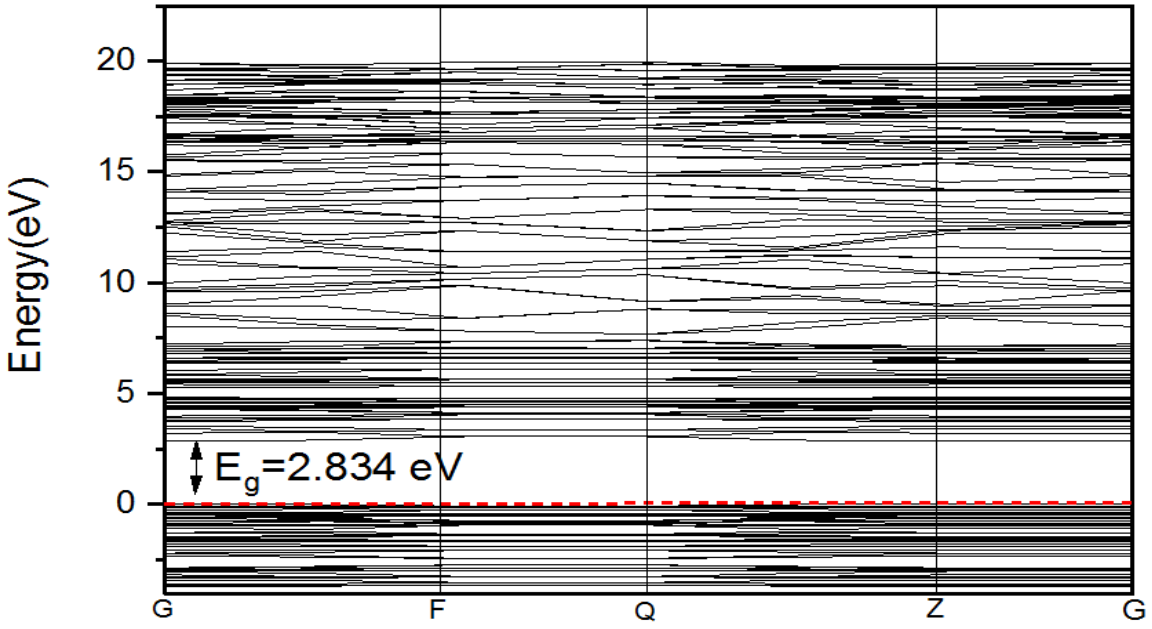

Figure 4.6: TiO_2 anatase (100) surface band structure

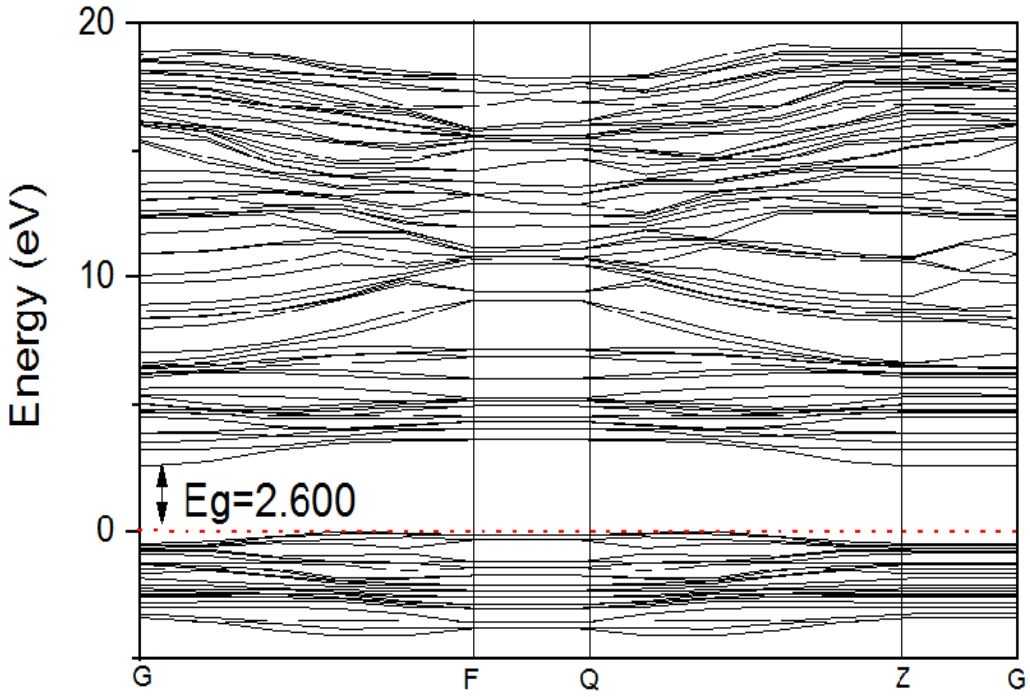

Figure 4.7: TiO_2 anatase (010) surface band structure

Figures 45, 4.6 and 4.7 give the electronic energy band structures for TiO_2 anatase bulk structure, (100) and (010) TiO_2 anatase surface respectively calculated using DFT. The red dashed lines indicate the Fermi energy level. The figures also illustrate the band gap of the two surfaces and of the bulk structure.

4.1.3.2. Density of State

The total density of states (TDOS) and partial density of states (PDOS) of bulk, (100) and (010) surfaces of anatase TiO_2 are shown in Figures 4.8, 4.9 and 4.10 respectively. The band gap is defined as the separation between the valence band and conduction band. The distance between Valence band and conduction band on the TDOS of anatase TiO_2 (100) and (010) TiO_2 becomes slightly wide compared to that of pure TiO_2, which indicates that the electronic non-locality is more obvious, owing to the reduction of crystal symmetry. The valence band mainly consists of O 2p states, and Ti 3d states are major composition for the conduction band for all the systems.

The density of state describes the number of available states per distance of energy at each energy state which can be occupied by electrons. A great PDOS at a given energy state means that there are numerous available states for occupation by electrons while a PDOS of zero represents that there are no states that can be occupied by electrons. The electron moves from the valence band of a semiconductor to the conduction band of a semiconductor, if there is no state for occupation then the electron falls back and cause charge recombination between the valence and conduction band of semiconductor.

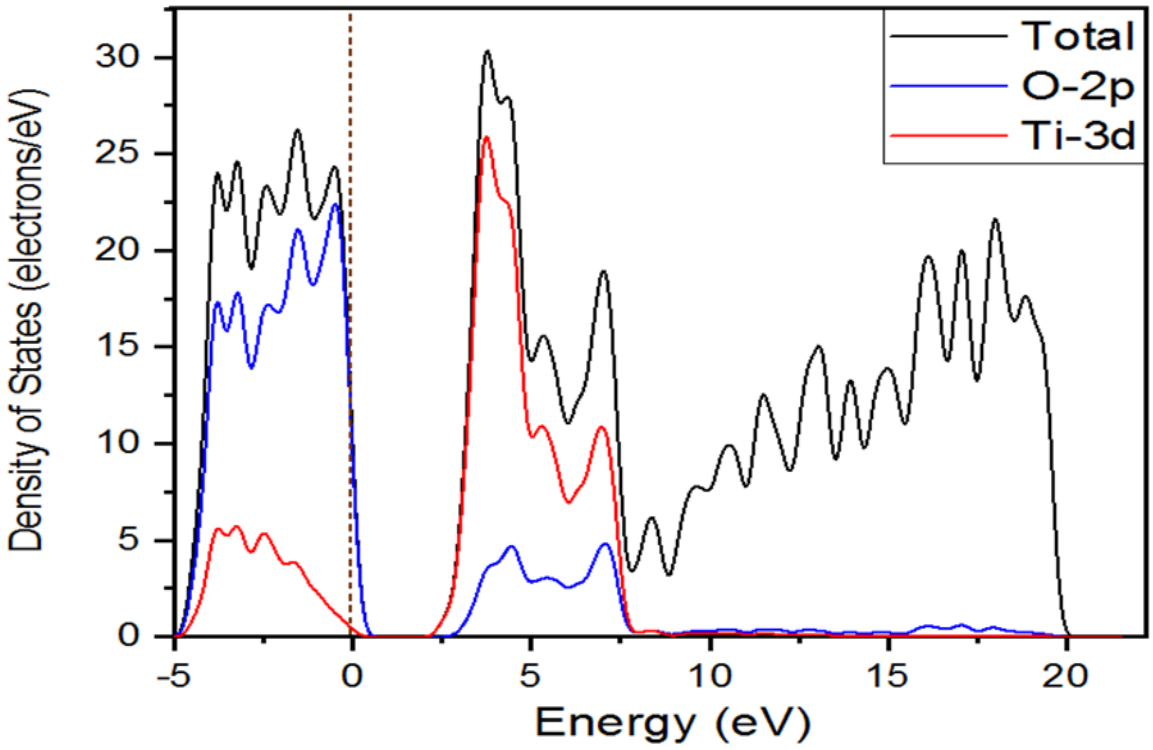

Figure 4.8: TiO_2 Bulk Structure anatase PDOS

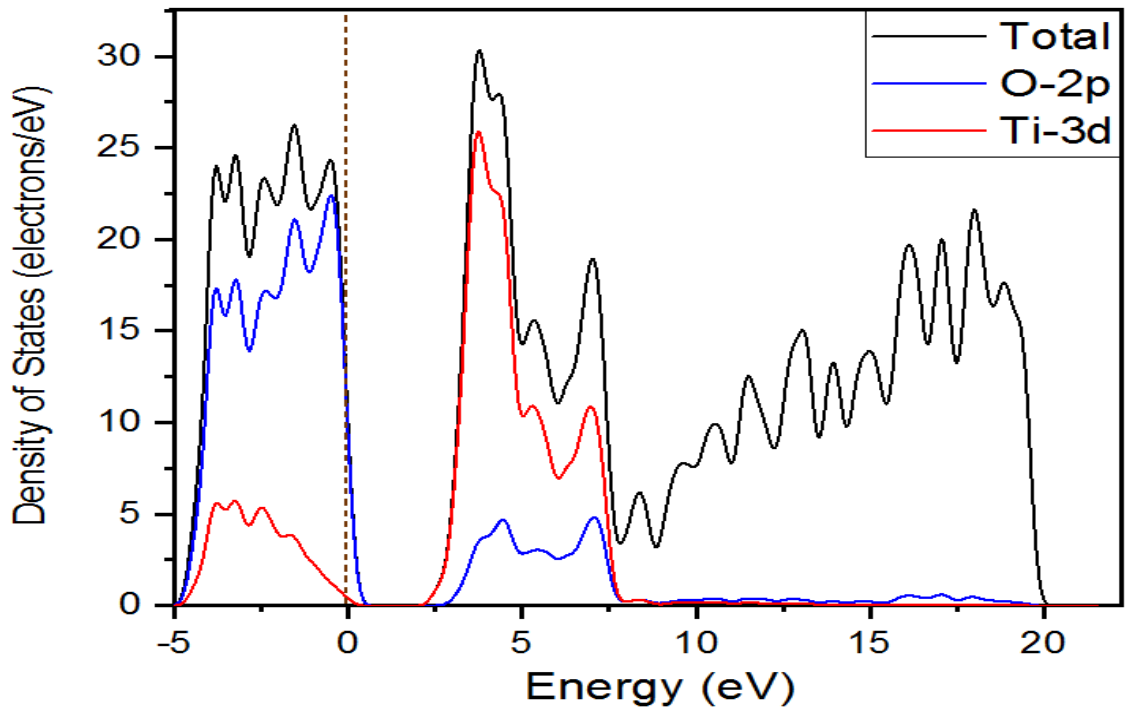

Figure 4.9: TiO_2 anatase (100) surface PDOS

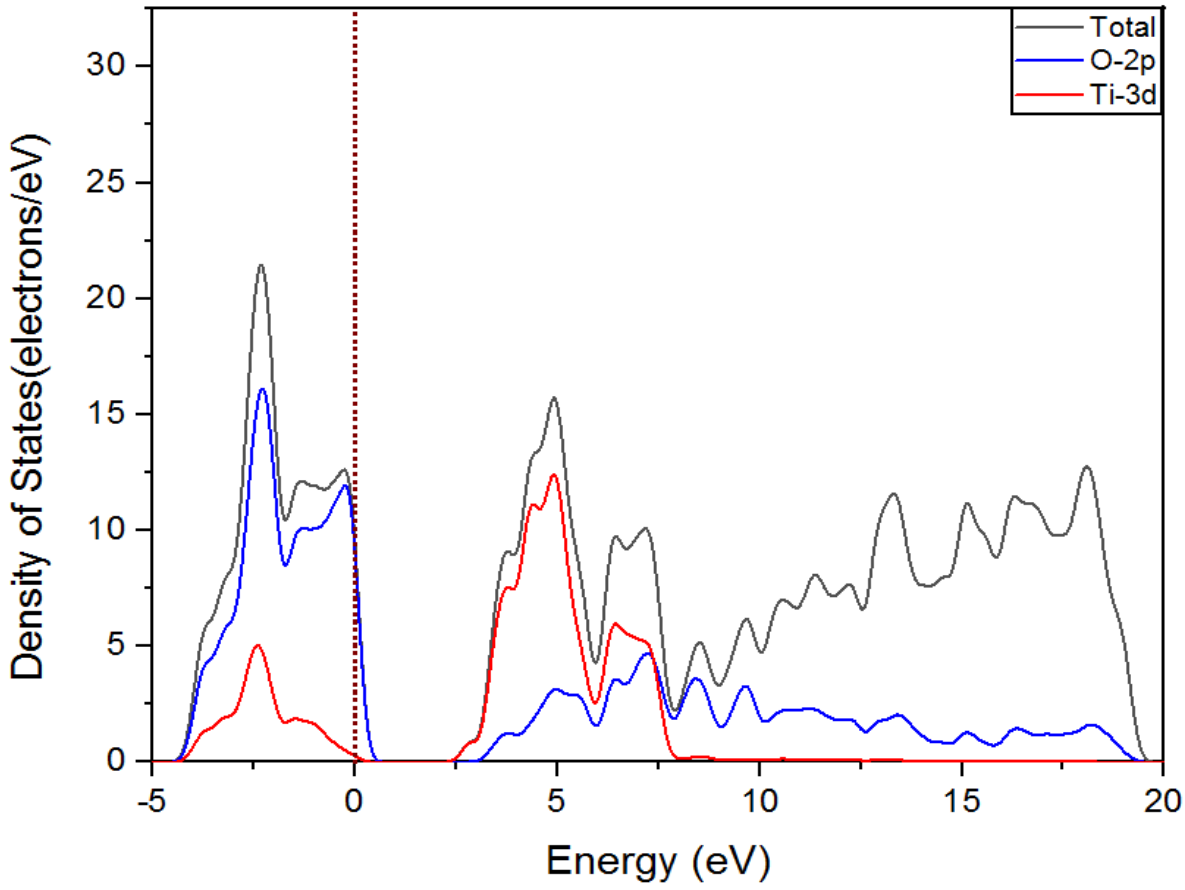

Figure 4.10: TiO_2 anatase (010) surface PDOS

As illustrated in figures it can be observed that TiO_2 anatase bulk structure, (100) and (010) TiO_2 anatase surface respectively has the state for electron occupation. TiO_2 anatase valence band and conduction band are mainly composed of O 2p, Ti 3d orbitals, respectively. The PDOS of bulk structure and two surfaces are slightly similar as are composed of same atoms (oxygen and titanium).

4.1.4. Optical Properties

The optical properties of a semiconductor can be defined as any property that involves the interaction between electromagnetic radiation or light and the semiconductor. The property depends mainly on the band gap of the semiconductor, the band gap is either a direct or an indirect band gap [61]. Direct band gaps are those that only need photon to excite an electron from valence band to conduction band while indirect band-gap semiconductor needs also a phonon (in addition to photon) to excite an electron from valence band to conduction band. Same for opposite case if electron is coming from conduction band to valence band then only photon is emitted in the case of direct band gap semiconductors while both photon and phonon both are emitted in indirect band gap semiconductor [63,64]. In this section optical properties of simulated TiO_2 systems are discussed.

4.1.4.1. Optical Reflectivity

The optical reflectivity is the effectiveness in reflecting radiant energy. It is the fraction of incident electromagnetic power that is reflected at an interface. The reflectance spectrum or spectral reflectance curve is the plot of the reflectance as a function of wavelength [62].

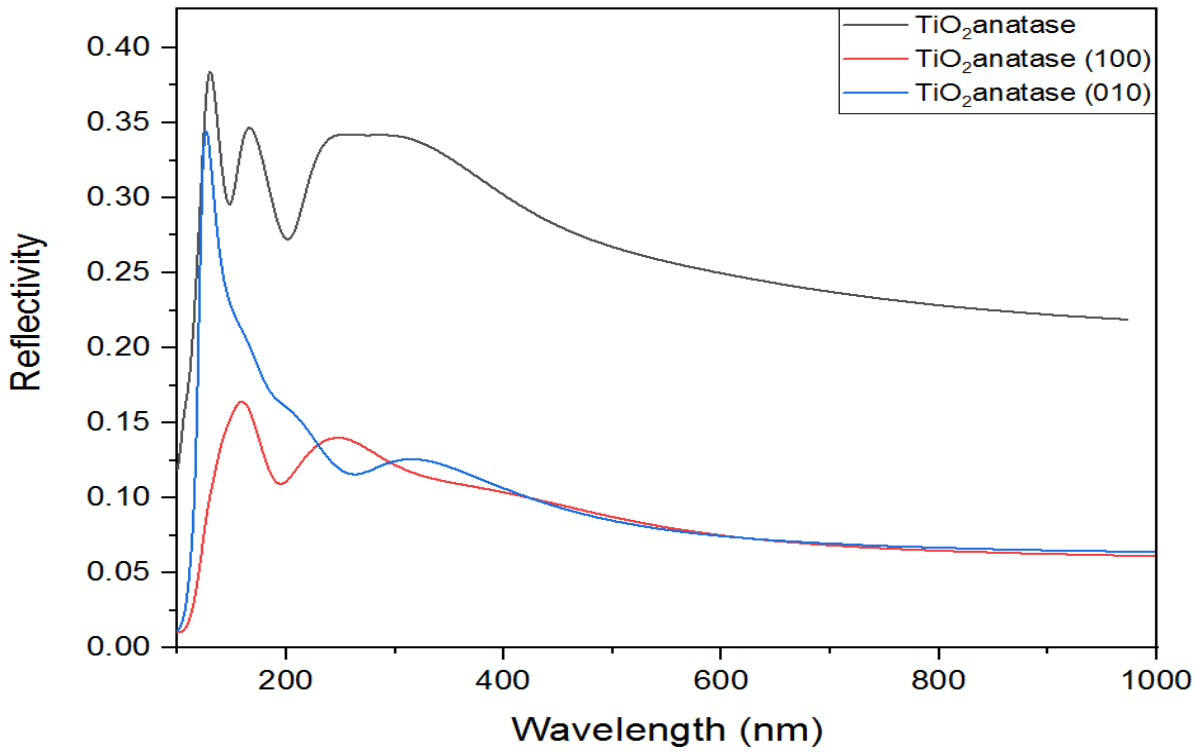

Figure 4.11: Optical reflectivity of anatase TiO_2, (100) and (010) anatase TiO_2 surface

The reflectivity of anatase TiO_2, (100) and (010) anatase TiO_2 surfaces in the wavelength ranges of 100 –1000 nm are illustrated on a Figure 4.11. The graph shows lower reflection of radiation on visible to near infrared region of solar spectrum for both surfaces, while the bulk system reflect more than (100) and (010) anatase TiO_2 surfaces. The lower reflection of radiation on the visible to near infrared region is due to re-orientation of atom while cleaving.

4.1.4.2. Optical Absorption

The energy of a photon can be transferred to an electron in the valence band of a semiconductor, which is brought to the conduction band, when the photon energy is larger than the band gap energy E_g. The photon is absorbed during this process and an electron–hole pair is generated [63, 64].

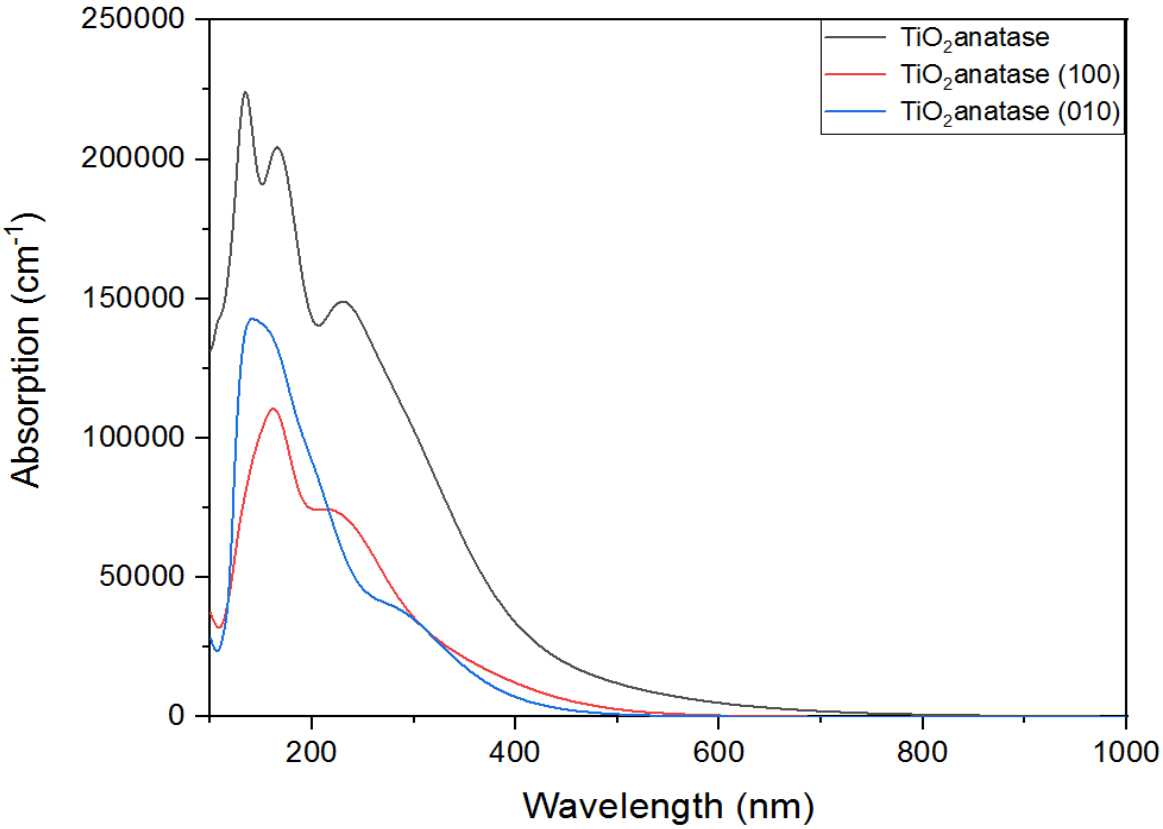

Figure 4.12: Optical absorption of anatase TiO_2, (100) and (010) anatase TiO_2 surface

The optical absorption coefficients for the TiO_2 anatase bulk structure, (100) and (010) anatase TiO_2 surfaces are compared in the figure 4.12. Experimentally the optical band gap is determine by excitation energy intercept at absorption edges in absorption spectra, optical band gap are quite different from those in electronic band gap. It is reasonable that the electronic band gap is based upon single particle approximation, while the optical absorption involves the excitation beyond single particle. The optical absorption of TiO_2 anatase bulk structure, (100) and (010) anatase TiO_2 surfaces shown in figure 4.13 shows that the bulk structure and surfaces can absorb photons on the ultra –violet region and towards near infrared region, since the figure 4.12 shows the stronger peaks in the ultraviolet region of solar spectrum, and weaker peaks in the visible to near infrared region of photons, below 50 000 cm^{-1}.

4.2. Croconate Dye Molecules (CR1 and CR2)

The two Croconate dye molecules CR1 and CR2 are depicted on Figure 4.13 CR1 contain electron donating methyl group (CH_3) which is an alkyl derived from methane, containing one carbon atom bonded to three hydrogen atoms while CR2 contain electron withdrawing carboxyl group (-COOH) which is an organic compound contained in carboxylic acid, one carbon atom bonded to two oxygen atoms and one hydrogen atom.

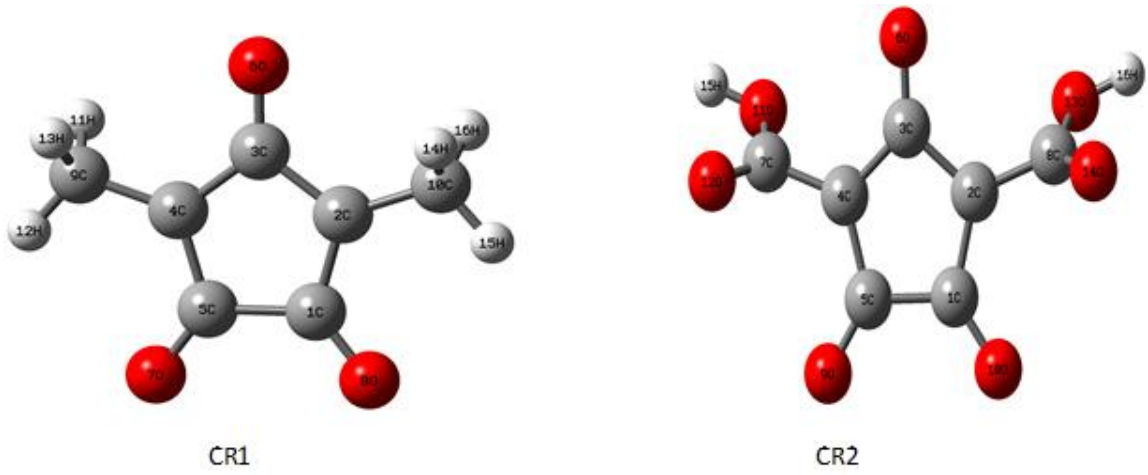

Figure 4.13: Croconate Dye molecules (CR1 and CR2)

The geometrical optimizations converged when the internal forces acting on all the atoms were less than $4.5x10^{-4}$ eV/A. The optimized geometry parameters: bond lengths and bond angles are presented in Table 4.2 The O6-C3 bond length of the oxyallyl moiety in CR1 is 1.236 Å, this is longer than the bond length of C5-O7/C1-C8 which is 1.220 Å. This was also the case for the bond length of O6-C3 (1.243 Å) and C5-O9/C1-O10 (1.238 Å) in CR2. The results suggest a more single bond character of the oxallyl compared to C5-O7/C1-C8 and C5-O9/C1-O10. Other findings obtained values of 1.299 Å O6-C3 bond length for the oxyallyl moiety and 1.213 Å for C5-O7/ C1-C8 in CR1, and O6-C3 (1.216 Å) and C5-O9/C1-O10 (1.208 Å) in CR2 [26], which are in good agreement with calculated results in this study.

Table 4.2: Optimized bond lengths of two models for croconate dyes, CR1 and CR2.

	O6 - C3(Å)	C3 – C4/C3 – C2 (Å)	C4 – R/C2 – R (Å)	C5 – O7/C1- O8. C5-O9/C1 – O10 (Å)
CR1	1.236	1.459	1.464	1.220
CR2	1.243	1.468	1.469	1.238

4.2.1. Excitation and Absorption Spectrum of the Dyes

UV-VIS absorption is a commonly used analytical tool for studying the interactions between electrons and radiation. On the other hand, infrared absorption is widely used to analyze the interactions between the vibration energy of bonds and electromagnetic waves.

Figure 4.15 illustrates UV-Vis spectra of the two dye molecules. The absorption maxima of CR1 is situated at 225 nm and 550 nm while the absorption peaks of CR2 are notably at 160 nm, 220 nm, 440 nm and 680 nm. The molecule CR2 demonstrates that more red shifted absorption than CR1, this may be as a result of the electron withdrawing carboxylic group in the structure of CR2. This suggests that the structure of CR1 and CR2 can be fine-tuned with the addition or substitution of chemical constituents to absorb more photon in the near infrared region.

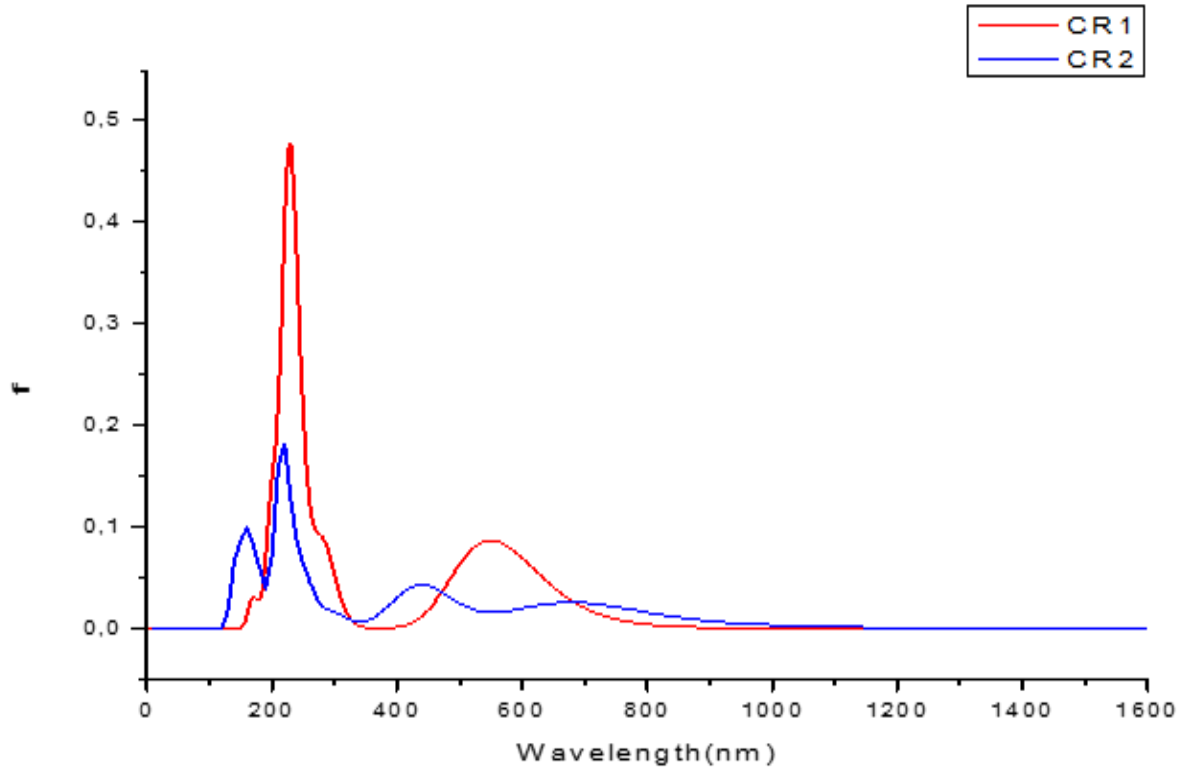

Figure 4.14: Calculated UV-Vis spectrum for CR1 and CR2 dye molecules.

4.2.2. Light Harvesting Efficiency of the Dyes

Light harvesting efficiency (LHE) plays an important role in improving the power conversion efficiency of DSSCs. LHE is defined as the fraction of light intensity absorbed by the dye at a certain wavelength in the DSSCs. Light harvesting efficiency for CR1 and CR2 at the absorption peaks was calculated using the equation:

$$\mathrm{LHE}(\lambda) = 1 - 10^{-\mathrm{f}} \tag{28}$$

where f denotes the absorption also called the oscillator strength of sensitizer at a given wavelength (λ).

Generally an increase in the LHE enhances the photocurrent response and thereby the efficiency of device. The LHE values of CR1 and CR2 calculated at their respective λ_{max} were found to be (0.661) 66.1 % at λ_{max} = 550 nm for CR1 and (0.339) 33.9% at λ_{max} = 680 nm for CR2. The LHE value of CR1 was 0.322 larger than that of CR2.

Therefore the dye CR1 is more efficient than CR2 in light harvesting. The LHE depends on the absorption (oscillator strength) at a known wavelength. The higher percentage of light harvesting efficiency of 66.1% was demonstrated by CR1 owing to its high oscillator strength at 225 nm

4.2.3. Optical Absorption of Dye Molecules.

The optical absorption of CR1 and CR2 croconate dye molecules are plotted and illustrated in Figure 4.15.

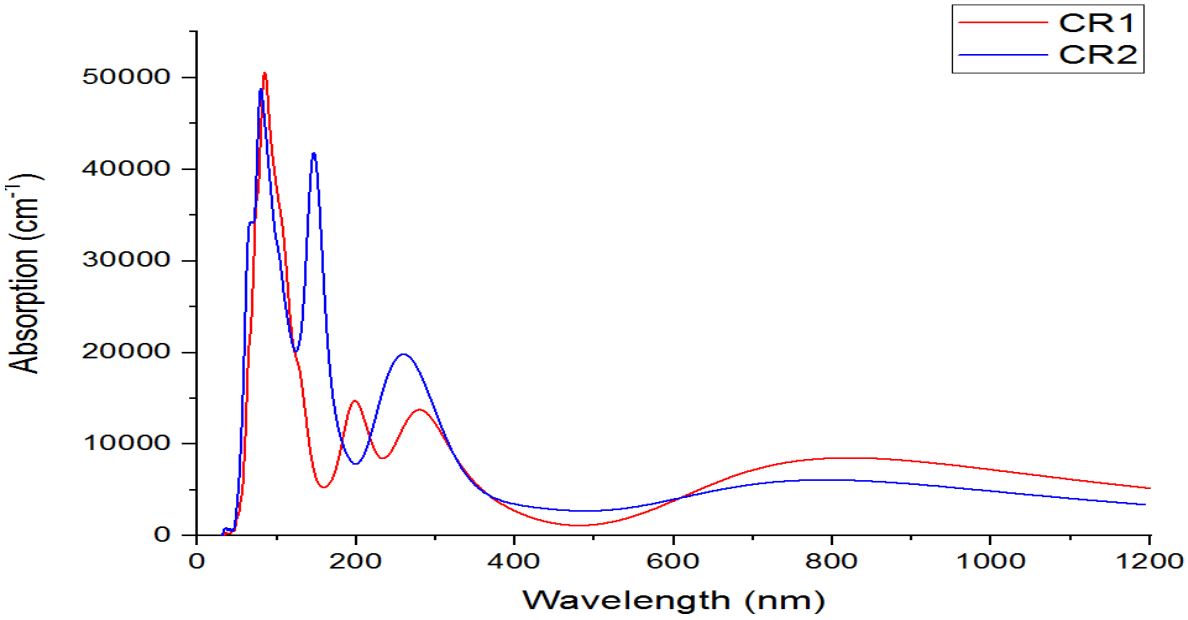

Figure 4.15: Calculated optical absorption for two dye molecules.

The graph reveals that both CR1 and CR2 dye molecules have a good absorption property. The optical absorption of CR1 and CR2 represented by the red and blue graphs respectively shows that the dye molecules absorbs intensely on the ultraviolet region and reveals a small absorption on the visible to near infrared region. A small absorption property for CR1 and CR2 is depicted by the absorption at 600 nm in the

infrared region. The absorption on the ultraviolet region for CR1 and CR2 are common for many sensitizers.

4.2.4. Energy Levels and Isodensity Surfaces of the Dyes

HOMO is the energy of the highest occupied molecular orbital of a molecule, LUMO is the energy of the lowest unoccupied molecular orbital of a molecule [64]. The isodensity surfaces of the dyes depicting the HOMO and LUMO of the dyes molecules are presented in Figure 4.17. The energy gap is generally the lowest energy electronic excitation that is possible in a molecule. The HOMO, LUMO and HOMO-LUMO energy gap of CR1 and CR2 dye molecules are presented in Table 4.3.

Table 4.3: The HOMO, LUMO and HOMO-LUMO energy gap of CR1 and CR2 dye molecules.

DYE MOLECULE	HOMO (eV)	LUMO (eV)	HOMO-LUMO GAP (eV)
CR1	-5.08	-7.49	2.32
CR2	-6.04	-8.08	2.04

The HOMO energies of CR1 and CR2 are −5.08 eV and −6.04 eV respectively while the LUMO energies of CR1 and CR2 were found to be −7.49 eV and −8.08 eV respectively. The HOMO–LUMO energy gap values for CR1 and CR2 were calculated to be 2.32 eV and 2.04 eV respectively and agrees well with the HOMO and LUMO values reported by Chitumalla et al [26] on Substituent effects on the croconate dyes in dye sensitized solar cell applications. The lower HOMO-LUMO energy gap of the sensitizer enhances absorption at higher wavelength and the photocurrent response of DSSCs. Low energy gap between the HOMO and LUMO of sensitizer enhances the absorption of photons in higher spectral regions of the solar spectrum. The two dyes relatively have low HOMO-LUMO energy gap, but the HOMO-LUMO energy gap of CR2 was lower than CR1, the lower HOMO-LUMO energy gap of CR2 suggest the red shifted absorption observed for CR2. The HOMO-LUMO energy gap and electronic band gap represents the minimum energy that is required to excite an electron up to a state in the conduction band where it can participate in conduction, energy must be input for electrons to become free, the practical performance of

DSSCs depend mostly on the band alignment, by adsorbing the molecules on the TiO2 semiconductor has an effect on the band alignment.

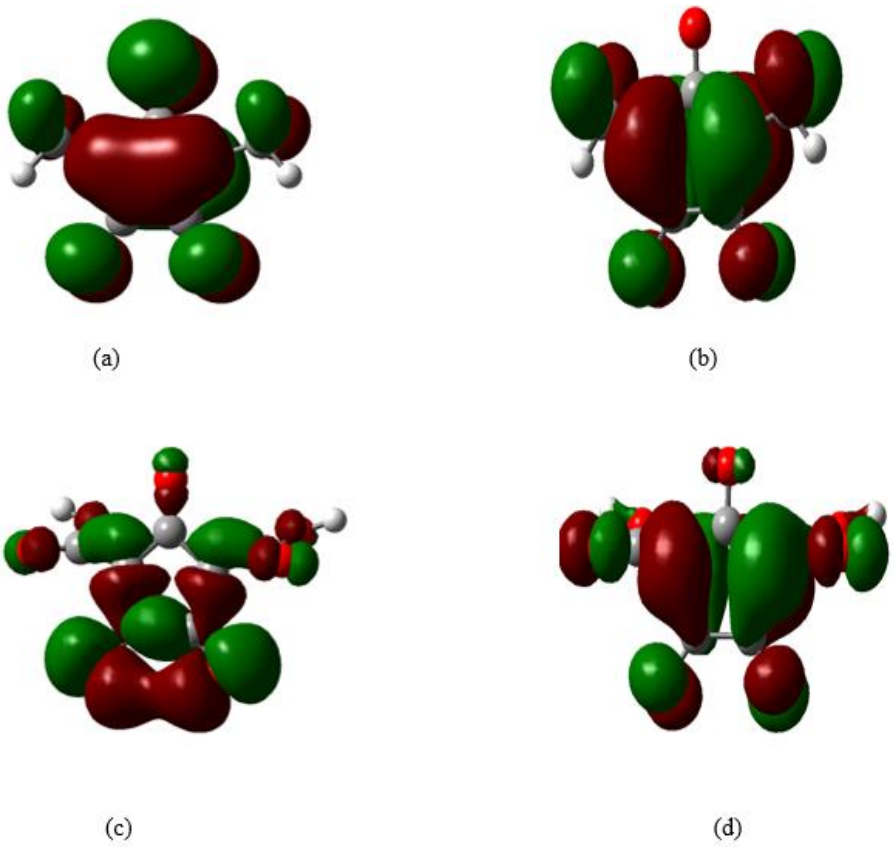

Figure 4.16: Isodensity surfaces of the molecular orbitals of (a) highest occupied molecular orbital of CR1 (b) lowest unoccupied molecular orbital of CR1 (c) highest occupied molecular orbital of CR2 (d) lowest unoccupied molecular orbital of CR2.

The HOMO of CR1 is delocalized on the oxyallyl group, and partly localized on the diketo group and electron donating methyl while the LUMO is delocalized on the carbon atoms of the cyclopentane and the methyl group. The HOMO of CR2 is delocalized on the diketo group and while the LUMO is delocalized on the carbon atoms of the cyclopentane. The different concentrations of the electron densities of HOMO and LUMO for CR1 and CR2 dyes molecules on this study suggest good electron transfer properties of the croconate dye molecules and agrees well with the the work done by Puyad *et al* [37] . The results imply that both CR1 and CR2 can

efficiently inject electron into the large band gap TiO_2 semiconductor and hence improve the overall performance of DSSCs.

4.3. TiO_2/Dye Complex

TiO_2/dye complex is the structure formed when the dye molecule is adsorbed on the surface of TiO_2, the substance being absorbed is an adsorbate and the absorbing substance, an adsorbent. In this study an adsorbate is a croconate dye molecules and the adsorbent is both (010 and 100) TiO_2 anatase.

Figures 4.17 and 4.18 shows shows Croconate CR1 adsorbed on (010 and 100) TiO_2 anatase and CR2 adsorbed on (010 and 100) TiO_2 anatase respectively to form the four TiO_2 /dye complexes that were investigated in this study.

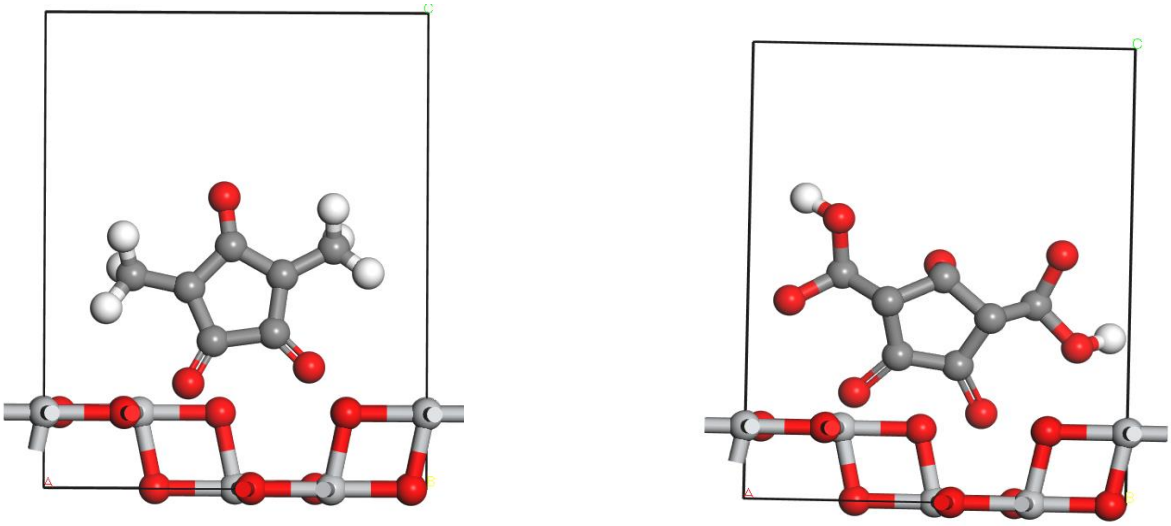

Anatase TiO_2 (010)/CR1 Anatase TiO_2 (010)/CR2

Figure 4.17: (100) anatase TiO_2 surface/dye complex

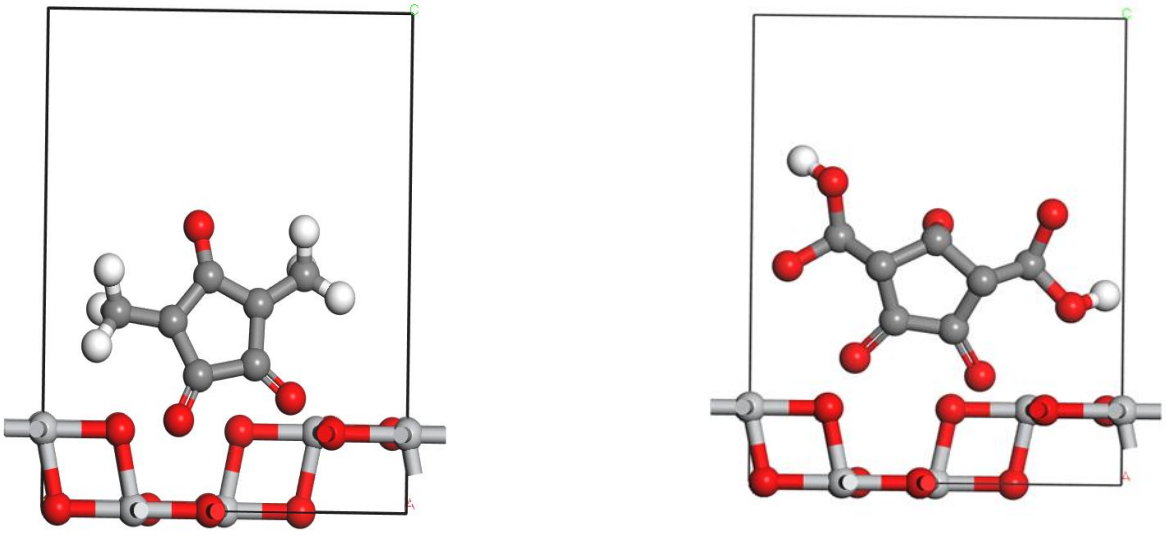

Anatase TiO_2 010/CR1 Anatase TiO_2 010/CR2

Figure 4.18: (010) anatase TiO_2 surface/dye complex

4.3.1. Electron Injection

After photo-excitation, the electron-hole separation, integral to the functioning of the cell, occurs by electron transfer from the photo-excited chromophore into the conduction band of the nanocrystalline semiconductor, in a time ranging from sub picoseconds to tens of picoseconds and even nanoseconds [64]. Efficient electron injection is fundamental for DSSCs operation, directly determines the short circuit current of the photovoltaic device. Electrons in excited states after photo-excitation, if not rapidly injected, easily lose the absorbed photon energy as heat through electron-phonon scattering and subsequent phonon dissipation thus generating (thermal) loss in efficiency. Therefore, it is of crucial importance to fully understand the interface electron transfer dynamics both experimentally and theoretically for further development of the nanoparticle-based device [65, 66].

The Φ_{inject} parameter reveal the presence of the electron injection efficiency and is related to the driving force ΔG_{inject} of electrons injecting from the excited states of dye molecules to the semiconductor substrate. It can be estimated by [66]:

$$\Delta G_{inject} = E_{OX}^{dye^*} - E_{CB}^{TiO_2} \quad (29)$$

where:

$E_{OX}^{dye^*}$ is the excited state oxidation potential of the dye.

$E_{CB}^{TiO_2}$ is the energy conduction band of the TiO_2 semiconductor (–4 eV).

Hence, $E_{OX}^{dye^*}$ can be determined using following equation:

$$E_{OX}^{dye^*} = E_{OX}^{dye} - \lambda_{max}^{ICT} \quad (30)$$

λ_{max}^{ICT} is the wavelength of maximum absorption for the lowest energy transition in the UV-Vis absorption spectrum of the dye molecules [32].

As the electron injection quantum yield Φ_{inject} from the excited dye molecules to the conduction band of the semiconductor increases, the performance of the DSSC improves, provided that this electron injection process is followed by efficient regeneration of the oxidized dye molecules by the electrolyte, such as the I^-/I^{3-} the redox couple [67].

Table 4.4: Electron injection between the dye molecules and (100) and (010) TiO_2 anatase.

Dye	$E_{OX}^{dye} -$	λ_{max}^{ICT}	$E_{CB}^{TiO_2}$	$E_{OX}^{dye^*}$	ΔG_{inject}
CR 1	-14108.804	0.47	-4.000	-14109.274	-14105.274
CR 2	-14420.442	0.18	-4.000	-14420.622	-14416.622

The calculated values of electron injection (ΔG_{inject}) shown in Table 4.4 show that E_{HOMO} lead to a significant decrease in the ΔG_{inject}. The negative values for ΔG_{inject} is an indication of spontaneous electron injection from the dye molecule to TiO_2, which is the requirement for efficient performance.

4.3.2. Adsorption Energy

The adsorption energy of TiO_2 /dye complex were calculated using the following equation [38]:

$$E_{ads} = \left(E_{TiO_2} + E_{dye}\right) - E_{TiO_2/dye} \quad (31)$$

where E_{ads} is the adsorption energy of TiO_2 /dye complex, E_{TiO_2} is the total energy of TiO_2 without adsorbed molecule, E_{dye} is the total energy of a dye molecule and $E_{TiO_2/dye}$ is the total energy of TiO_2 with adsorbed molecule.

Table 4.5: Adsorption energy between the dye molecule and (100) and (010) TiO_2 anatase

Surface	Dye	*E (ads)* (Kcal/mol)
(100)	CR 1	28.030
(100)	CR 2	29.104
(010)	CR 1	24.512
(010)	CR 2	26.931

The calculated adsorption energy illustrated in the Table 4.5 the positive value of $E\ (ads)$ shows that the TiO_2/dye surfaces complex are stable. The TiO_2/dye complex with higher adsorption enegy values is the most stable system, from Table 4.5 the calculated values of $E\ (ads)$ shows that TiO_2/CR2 complex is more stable than TiO_2/CR1 complex. Therefore CR2 binds strongly in both surfaces when compared to CR1. Puyad *et al.* [37] reported that the dye molecules with an electron-donating methyl group bind more strongly to the surface than the one with an electron-withdrawing carboxyl group. This consistent with croconate dye with a carboxyl substituent binds more strongly to the surface than the dye with methyl substituent. Thus, the adsorption strength increases with increasing electron donating power of substituent. The adsorption energies found on this studies are comparable with adsorption energies reported by Puyad et al [37] on the adsorption of croconate dyes on TiO_2 anatase (101) surface.

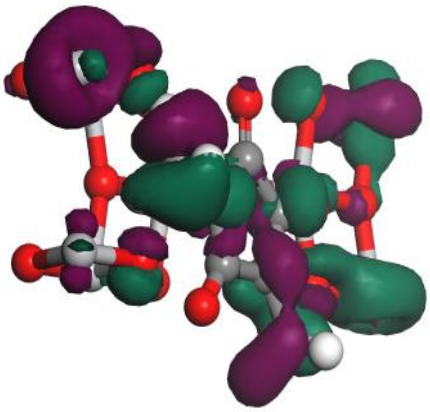

(a)

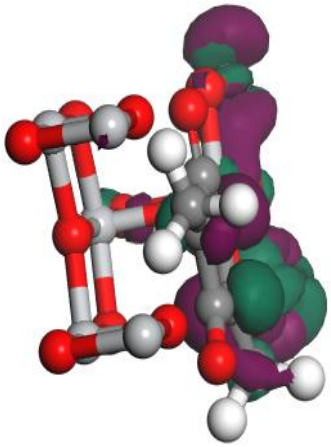

(b)

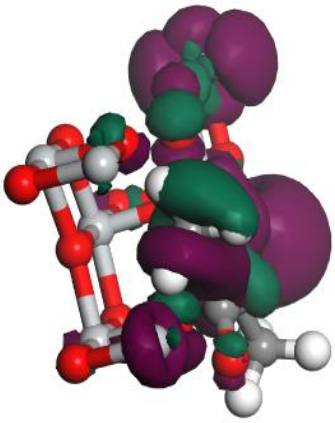

(c)

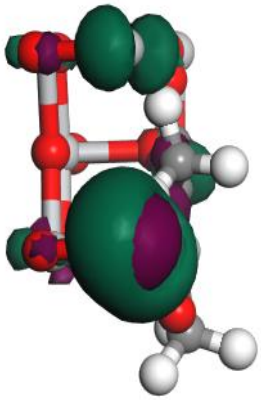

(d)

Figure 4.19: Isodensity surfaces of the molecular orbitals of (a) highest occupied molecular orbital of anatase TiO_2 (100)/CR1 complex (b) lowest unoccupied molecular orbital of anatase TiO_2 (100)/CR1 complex (c) highest occupied molecular orbital of anatase TiO_2 (100)/CR2 (d) lowest unoccupied molecular orbital of anatase TiO_2 (100)/CR2.

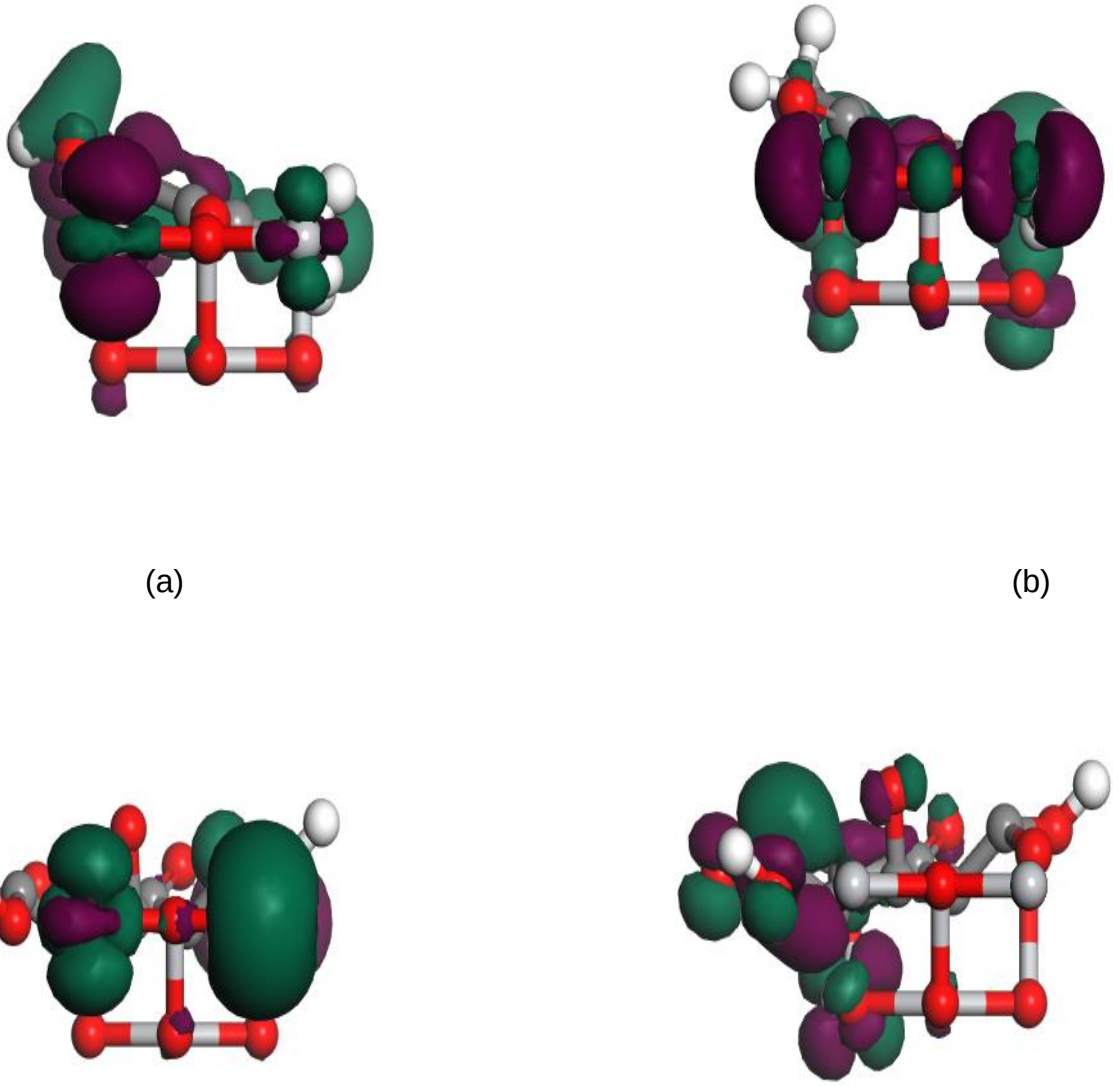

(a) (b)

(c) (d)

Figure 4.20: Isodensity surfaces of the molecular orbitals of (a) highest occupied molecular orbital of anatase TiO_2 (010)/CR1 complex (b) lowest unoccupied molecular orbital of anatase TiO_2 (010)/CR1 complex (c) highest occupied molecular orbital of anatase TiO_2 (010)/CR2 (d) lowest unoccupied molecular orbital of anatase TiO_2 (010)/CR2.

The isodensity surfaces of the molecular orbitals for the TiO_2/ dye complex structures are presented in Figures 4.20 and 4.21. The calculated results show that after adsorption the LUMO level decreases due to the interaction with TiO_2. The LUMO of TiO_2/ dye complex is now located above the conduction band of TiO_2 (~ - 4.000 eV) and also demonstrated that deprotonation of dye leads to the HOMO being inside the band gap of TiO_2.

CONCLUSSION

Density functional theory approach has being successful applied to investigate the adsorption of two model croconate dye one with electron donating methyl group (CR1) and other with electron carboxyl group (CR2) on (010 and 100) anatase TiO_2 surface. The generalized gradient approximation (GGA) was used in the scheme of Perdew-Burke Ernzerhof to describe the exchange-correlation functions of the systems. The calculations were carried using VAMP and CASTEP code as implemented in material studio of BIOVIA inc.

The main objective set for this study achieved, and the results shows that the HOMO and LUMO energy levels of CR1 and CR2 dye obtained satisfies main requirement for efficient electron injection with the LUMO level higher than the conduction band of anatase TiO_2 and the HOMO level sufficiently lower than the redox couple. The UV-Vis absorption spectra revealed that CR1 and CR2 dye molecules exhibits broader adsorption indicating its ability to absorb wider energy range in the visible region, the optical absorption of dyes shows a broad absorption activity on the visible and near infrared region of solar spectrum which gives evidence that adsorbing these dye molecules to an anatase TiO_2 semiconductor will shift the absorption of photons from ultraviolet to visible and near infrared region of solar spectrum.

The electron injection efficiency which is related to the driving force ΔG_{inject} and the adsorption energy between dye molecules and TiO_2 semiconductor were studied and the results shows a spontaneous electron injection, the adsorption energy points out to large values which shows that the complexes are stable and strong binding ability of CR2 to the TiO_2 surface, but also shows a comparable binding strength of CR1.

REFERENCES

[1] Trollip, H., Butler, A., Burton, J., Caetano, T., & Godinho, C. (2014). Energy Security in South Africa.

[2] Eisenberg, R., & Nocera, D. G. (2005). Preface: Overview of the forum on solar and renewable energy. Inorganic Chemistry, 44(20), 6799-6801.

[3] Chopra, K. L., Paulson, P. D., & Dutta, V. (2004). Thin-film solar cells: an overview. Progress in Photovoltaics: Research and Applications, 12(2-3), 69-92.

[4] Yamamoto, T., Yamashita, F., Tanaka, I., Matsubara, E., & Muramatsu, A. (2004). Electronic states of sulfur doped TiO_2 by first principles calculations. Materials transactions, 45(7), 1987-1990.

[5] Bagher, A. M., Vahid, M. M. A., & Mohsen, M. (2015). Types of solar cells and application. American Journal of Optics and Photonics, 3(5), 94-113.

[6] Martsinovich, N., Jones, D. R., & Troisi, A. (2010). Electronic structure of TiO_2 surfaces and effect of molecular adsorbates using different DFT implementations. The Journal of Physical Chemistry C, 114(51), 22659-22670.

[7] Wang, Y., Zhang, R., Li, J., Li, L., & Lin, S. (2014). First-principles study on transition metal-doped anatase TiO_2. Nanoscale research letters, 9(1), 46.

[8] Sorrell, C. A. (2001). Rocks and minerals: A guide to field identification. Macmillan.

[9] Fujishima, A., Rao, T. N., & Tryk, D. A. (2000). Titanium dioxide photocatalysis. Journal of photochemistry and photobiology C: Photochemistry reviews, 1(1), 1-21.

[10] Chen, C., Ma, W., & Zhao, J. (2010). Photocatalytic degradation of organic pollutants by co-doped TiO_2 under visible light irradiation. *Current Organic Chemistry*, *14*(7), 630-644.

[11] Jasim, K. E. (2011). Dye sensitized solar cells-working principles, challenges and opportunities. In Solar Cells-Dye-Sensitized Devices. InTech.

[12] Kohn, W., & Sham, L. J. (1965). Self-consistent equations including exchange and correlation effects. Physical Review, 140(4A), A1133.

[13] Ceperley, D. M., & Alder, B. J. (1980). Ground state of the electron gas by a stochastic method. Physical Review Letters, 45(7), 566.

[14] Trabelsi, K., Hajjaji, A., Gaidi, M., Bessais, B., & El Khakani, M. A. (2017). Enhancing the photoelectrochemical response of TiO_2 nanotubes through their nanodecoration by pulsed-laser-deposited Ag nanoparticles. Journal of Applied Physics, 122(6), 064503..

[15] Zimmermann, H. (2000). Basics of optical emission and absorption. In Integrated Silicon Optoelectronics (pp. 1-10). Springer, Berlin, Heidelberg.

[16] AP Ribeiro, R., R de Lazaro, S., & R de Oliveira, C. (2016). Band-Gap Engineering for Photocatalytic Applications: Anionic and Cationic Doping of TiO_2 Anatase. Current Physical Chemistry, 6(1), 22-27.

[17] Dayal, S., Kopidakis, N., Olson, D. C., Ginley, D. S., & Rumbles, G. (2009). Photovoltaic devices with a low band gap polymer and CdSe nanostructures exceeding 3% efficiency. Nano letters, 10(1), 239-242.

[18] Assadi, M. H. N., & Hanaor, D. A. (2013). Theoretical study on copper's energetics and magnetism in TiO_2 polymorphs. Journal of Applied Physics, 113(23), 233913.

[19] Han, Y. X., Yang, C. L., Wang, M. S., Ma, X. G., & Wang, L. Z. (2015). Enhancing the visible-light absorption of TiO_2 with the use of key N, Co, and Na dopant concentrations. Solar Energy Materials and Solar Cells, 132, 94-100.

[20] de Lazaro, S. R., Ribeiro, R. A. P., & da Silveira Lacerda, L. H. (2017). Quantum Chemistry Applied to Photocatalysis with TiO_2. In *Titanium Dioxide*. InTech.

[21] Long, R., & English, N. J. (2009). Band gap engineering of (N, Ta)-codoped TiO_2: A first-principles calculation. Chemical Physics Letters, *478*(4-6), 175-179...

[22] Jensen, S., & Kilin, D. (2013). Electronic Properties of Silver Doped TiO_2 Anatase (100) Surface. Nanotechnology for Sustainable Energy, 1140, 187-218.

[23] Wang, J., Tafen, D. N., Lewis, J. P., Hong, Z., Manivannan, A., Zhi, M. ... & Wu, N. (2009). Origin of photocatalytic activity of nitrogen-doped TiO_2 nanobelts. Journal of the American Chemical Society, 131(34), 12290-12297...

[24] Meng, S., Kaxiras, E., Nazeeruddin, M. K., & Grätzel, M. (2011). Design of dye acceptors for photovoltaics from first-principles calculations. The Journal of Physical Chemistry C, 115(18), 9276-9282.

[25] Triggiani, L., Muñoz-García, A. B., Agostiano, A., & Pavone, M. (2015). First-principles study of trimethylamine adsorption on anatase TiO_2 nanorod surfaces. Theoretical Chemistry Accounts, 134(10), 119.

[26] Chitumalla, R. K., Lim, M., Gao, X., & Jang, J. (2015). Substituent effects on the croconate dyes in dye sensitized solar cell applications: a density functional theory study. Journal of Molecular Modeling, 21(11), 297.

[27] Li,S.L.,Jiang,K.J.,Shao,K.F.,& Yang,L.M. (2006). Novel Organic dyes for efficient dye-sensitized solar cells. Chemical Communications, (26), 2792-2794

[28] Bienfait, B., & Ertl, P. (2013). JSME: a free molecule editor in JavaScript. Journal of Cheminformatics, 5(1), 24.

[29] Rego, N., & Koes, D. (2014). 3Dmol. js: molecular visualization with WebGL. Bioinformatics, 31(8), 1322-1324.

[30] Lee, C. P., Li, C. T., & Ho, K. C. (2017). Use of organic materials in dye-sensitized solar cells. Materials Today, 20(5), 267-283.

[31] Marcano, E. (2018). DFT Study of Anthocyanidin and Anthocyanin Pigments for Dye Sensitized Solar Cells: Electron Injecting from the Excited States and Adsorption onto TiO_2 (Anatase) Surface. Energy Harvesting and Systems, 5(1-2), 29-38.

[32] Oprea, C. I., Panait, P., Lungu, J., Stamate, D., Dumbravă, A., Cimpoesu, F., & Gîrţu, M. A. (2013). DFT study of binding and electron transfer from a metal-free dye with carboxyl, hydroxyl, and sulfonic anchors to a titanium dioxide nanocluster. International Journal of Photoenergy, 2013.

[33] De Angelis, F. (2010). Direct vs. indirect injection mechanisms in perylene dye-sensitized solar cells: A DFT/TDDFT investigation. Chemical Physics Letters, 493(4-6), 323-327.

[34] Anderson, S., Constable, E. C., Dare-Edwards, M. P., Goodenough, J. B., Hamnett, A., Seddon, K. R., & Wright, R. D. (1979). Chemical modification of a titanium (IV) oxide electrode to give stable dye sensitisation without a supersensitiser. Nature, 280(5723), 571.

[35] Lundqvist, M. J., Nilsing, M., Persson, P., & Lunell, S. (2006). DFT study of bare and dye-sensitized TiO_2 clusters and nanocrystals. International Journal of Quantum Chemistry, 106(15), 3214-3234.

[36] Niu, M. (2017). The Adsorption Geometry and Electronic Structure of Organic Dye Molecule on TiO_2 (101) Surface from First Principles Calculations. In MATEC Web of Conferences (Vol. 88, p. 03002). EDP Sciences.

[37] Puyad, A. L., Kumar, C. R., & Bhanuprakash, K. (2012). Adsorption of croconate dyes on TiO_2 anatase (101) surface: A periodic DFT study to understand the binding of diketo groups. Journal of Chemical Sciences, 124(1), 301-310.

[38] Krieger, J. B., Li, Y., & Iafrate, G. J. (1990). Derivation and application of an accurate Kohn-Sham potential with integer discontinuity. Physics Letters A, 146(5), 256-260.

[39] Krieger, J. B., Li, Y., & Iafrate, G. J. (1992). Accurate local spin-polarized exchange potential: Reconciliation of generalized Slater and Kohn–Sham methods. International journal of quantum chemistry, 41(3), 489-496.

[40] Jensen, F. (2013). Atomic orbital basis sets. Wiley Interdisciplinary Reviews: Computational Molecular Science, 3(3), 273-295.

[41] Davidson, E. R., & Feller, D. (1986). Basis set selection for molecular calculations. Chemical Reviews, 86(4), 681-696.

[42] Ditchfield, R. H. W. J., Hehre, W. J., & Pople, J. A. (1971). Self-consistent molecular-orbital methods. IX. An extended Gaussian-type basis for molecular-orbital studies of organic molecules. The Journal of Chemical Physics, 54(2), 724-728.

[43] Schwerdtfeger, P. (2011). The pseudopotential approximation in electronic structure theory. The Journal of Chemical Physics, 12(17), 3143-3155.

[44] Louie, S. G., Froyen, S., & Cohen, M. L. (1982). Nonlinear ionic pseudopotentials in spin-density-functional calculations. Physical Review B, 26(4), 1738.

[45] Reis, C. L., Pacheco, J. M., & Martins, J. L. (2003). First-principles norm-conserving pseudopotential with explicit incorporation of semicore states. Physical Review B, 68(15), 155111.

[46] Hamann, D. R., Schlüter, M., & Chiang, C. (1979). Norm-conserving pseudopotentials. Physical Review Letters, 43(20), 1494.

[47] Bachelet, G. B., Hamann, D. R., & Schlüter, M. (1982). Pseudopotentials that work: From H to Pu. Physical Review B, 26(8), 4199.

[48] Vanderbilt, D. (1990). Soft self-consistent pseudopotentials in a generalized eigenvalue formalism. Physical Review B, 41(11), 7892.

[49] Kresse, G., & Joubert, D. (1999). From ultrasoft pseudopotentials to the projector augmented-wave method. Physical Review B, 59(3), 1758.

[50] Thomson, K. T., & Wentzcovitch, R. M. (1998). A density functional study of the electronic structure of sodalite. The Journal of chemical physics, 108(20), 8584-8588.

[51] Inoue, K., & Ohtaka, K. (2004). Photonic crystals: physics, fabrication and applications. Springer Science & Business Media, 94

[52] Baekelandt, B. G., Cedillo, A., & Parr, R. G. (1995). Reactivity indices and fluctuation formulas in density functional theory: isomorphic ensembles and a new measure of local hardness. The Journal of chemical physics, 103(19), 8548-8556.

[53] Theivasanthi, T., & Alagar, M. (2013). Titanium dioxide (TiO_2) nanoparticles XRD Analyses: An Insight. arXiv preprint arXiv:1307.1091.

[54] Ohsaka, T., Izumi, F., & Fujiki, Y. (1978). Raman spectrum of anatase, TiO_2. Journal of Raman Spectroscopy, 7(6), 321-324.

[55] Car, R., de Angelis, F., Giannozzi, P., & Marzari, N. (2005). First-principles molecular dynamics. In Handbook of Materials Modeling (pp. 59-76). Springer, Dordrecht.

[56] Thygesen, K. S., & Jacobsen, K. W. (2005). Interference and k-point sampling in the supercell approach to phase-coherent transport. Physical Review B, 72(3), 033401.

[57] Buckland, S. T., Anderson, D., Burnham, K., Laake, J., Thomas, L., & Borchers, D. (2001). Introduction to distance sampling: estimating abundance of biological populations (Vol. 335). Oxford: Oxford University Press.

[58] Blöchl, P. E., Jepsen, O., & Andersen, O. K. (1994). Improved tetrahedron method for Brillouin-zone integrations. Physical Review B, *49*(23), 16223.

[59] Benam, M. R. (2011). First Principles Studies of the Effect of Nitrogen Impurities on the Energy Gap of Rutile Ti0$_2$ïNxby Pseudopotential Approaches. Journal of Engineering and Applied Sciences, 6(1), 18-20.

[60] Chen, G. (2005). Nanoscale energy transport and conversion: a parallel treatment of electrons, molecules, phonons, and photons. Oxford University Press.

[61] Henglein, A. (1989). Small-particle research: physicochemical properties of extremely small colloidal metal and semiconductor particles. Chemical Reviews, 89(8), 1861-1873.

[62] Splendiani, A., Sun, L., Zhang, Y., Li, T., Kim, J., Chim, C. Y. ... & Wang, F. (2010). Emerging photoluminescence in monolayer MoS_2. Nano Letters, 10(4), 1271-1275.

[63] McIntyre, J. D. E., & Aspnes, D. E. (1971). Differential reflection spectroscopy of very thin surface films. Surface Science, 24(2), 417-434.

[64] Pearson, R. G. (1986). Absolute electronegativity and hardness correlated with molecular orbital theory. Proceedings of the National Academy of Sciences, 83(22), 8440-8441.

[65] Ma, W., Zhang, F., & Meng, S. (2014). Atomic Scale Investigation of Dye Sensitized Solar Cells_Interface Structure and Dynamics. arXiv preprint arXiv:1406.3111.

[66] Kalyanasundaram, K., & Grätzel, M. (1997). Photovoltaic performance of injection solar cells and other applications of nanocrystalline oxide layers. Journal of Chemical Sciences, 109(6), 447-469.